CrossMark

J. Fluid Mech. (2015), *vol.* 781, *pp.* 353–387. © Cambridge University Press 2015
doi:10.1017/jfm.2015.503

A boundary layer model for ice stream margins

M. Haseloff[1,†], C. Schoof[1] and O. Gagliardini[2,3,4]

[1]Department of Earth, Ocean and Atmospheric Sciences, University of British Columbia, Vancouver, BC V6T 1Z4, Canada

[2]CNRS, LGGE, UMR5183, 38041 Grenoble, France

[3]Université de Grenoble Alpes, LGGE, UMR5183, 38041 Grenoble, France

[4]Institut Universitaire de France, Paris, France

(Received 16 February 2015; revised 3 August 2015; accepted 24 August 2015; first published online 18 September 2015)

The majority of Antarctic ice is discharged via long and narrow fast-flowing ice streams. At ice stream margins, the rapid transition from the vertical shearing flow in the ice ridges surrounding the stream to a rapidly sliding plug flow in the stream itself leads to high stress concentrations and a velocity field whose form is non-trivial to determine. In this paper, we develop a boundary layer theory for this narrow region separating a lubrication-type ice ridge flow and a membrane-type ice stream flow. This allows us to derive jump conditions for the outer models describing ridge and stream self-consistently. Much of our focus is, however, on determining the velocity and shear heating fields in the margin itself. Ice stream margins have been observed to change position over time, with potentially significant implications for ice stream discharge. Our boundary layer model allows us to extend previous work that has determined rates of margin migration from a balance between shear heating in the margin and the cooling effect of margin migration into the colder ice of the surrounding ice ridge. Solving for the transverse velocity field in the margin allows us to include the effect of advection due to lateral inflow of ice from the ridge on margin migration, and we demonstrate that this reduces the rate of margin migration, as previously speculated.

Key words: boundary layers, geophysical and geological flows, ice sheets

1. Introduction

Ice streams are narrow regions of fast ice flow that stretch from the margin of a continental ice sheet into its interior. The flow velocities of ice streams can exceed those of the surrounding, slowly flowing parts of the ice sheet by orders of magnitude, making them stand out prominently in velocity maps (Rignot, Mouginot & Scheuchl 2011). In present-day ice sheets, ice streams are especially prevalent in Antarctica, where they account for a significant fraction of total ice discharge from the continent.

Ice streams present a particular challenge to ice sheet models, in that the mechanics of ice stream flow are often quite different from those of the remainder of the ice sheet (Schoof & Hewitt 2013). Rather than flowing as shearing flows in the style

† Email address for correspondence: mhaseloff@eos.ubc.ca

https://doi.org/10.1017/jfm.2015.503 Published online by Cambridge University Press

of other geophysical gravity currents (Huppert 1982), ice streams often flow as plug flows in which extensional and lateral stresses are significant (Joughin *et al.* 2002). Different leading-order thin-film models are appropriate to ice streams and to the areas of slow flow (termed ice ridges) between them. Early studies of the coupled flow of ice streams and ice ridges typically used so-called 'shallow ice' models for the shearing flow in the ridges (Fowler & Larson 1978; Morland & Johnson 1980) and membrane-type 'shallow stream' models for the ice streams (MacAyeal 1989). The coupling between these is, however, generally formulated on an *ad hoc* basis, as is the case, for instance, in the pioneering work of Hulbe & MacAyeal (1999).

In cases where the transition from stream flow to ridge flow is abrupt, the thin-film approximations behind 'shallow ice' and 'shallow stream' must fail, and a boundary layer description becomes necessary to capture the coupling between slowly and rapidly flowing ice. The relevant jump conditions between ridge and stream models should then be dictated by that boundary layer. The need for a boundary layer persists in principle even for the nowadays widely used 'higher-order' models of ice sheet flow that generalize shearing- and membrane-type flows into a single mathematical description (Pattyn 2003; Kyrke-Smith, Katz & Fowler 2013). Despite their versatility in describing slow shearing flows as well as rapid flows dominated by extensional and lateral stresses, these higher-order models are still only appropriate for thin films (Schoof & Hindmarsh 2010) and cannot accurately capture abrupt transitions between slow and fast flow.

The purpose of this paper is to develop the relevant model for such a transition through the use of matched asymptotic expansions. In the process, we re-derive the relevant 'outer' models for ice ridge and ice stream flow, but our main purpose is to arrive at a consistent way of coupling the two through a boundary layer. We assume that ice streams and ice ridges are not only shallow, but also narrow in plan view, being much longer in the along-flow direction than they are wide, and focus on the boundary layer that forms the lateral margin of an ice stream.

Our boundary layer model provides the appropriate jump conditions that couple the leading-order outer flow models at the ridge–stream boundary. By allowing the velocity structure in the boundary layer itself to be solved for, it further allows us to derive a self-consistent description of temperature in the ice stream margin, building on previous attempts that have either ignored the effect of advection by lateral flow through the margin (Schoof 2004, 2012) or parameterized it (Jacobson & Raymond 1998; Suckale *et al.* 2014). If we assume that the switch from slow flow to fast flow corresponds to a change in basal temperature from ice that is frozen to the bed to a bed that is at the melting point (e.g. Payne & Dongelmans 1997), then solving for temperature becomes key to determining the rate of margin migration over time. Here, we use the mechanical component of our margin boundary layer to extend the model for the thermally driven migration of shear margins due to heat dissipation in Schoof (2012). This allows the boundary between stream and ridge flow to be treated as a free boundary, which observations suggest is a necessary component of modelling coupled stream–ridge systems (e.g. Echelmeyer & Harrison 1999; Conway *et al.* 2002; Catania *et al.* 2012).

The paper is organized as follows: in § 2, we lay out the basic ice flow model. We then non-dimensionalize the model and derive its leading-order versions appropriate to stream and ridge flow in §§ 3 and 4, paying particular attention to how the relevant scales in the ridge are related to those in the stream. We use these to develop a leading-order model for the boundary layer in § 5, and we apply asymptotic matching to couple the different regions together in § 6. Note that a brief guide to the non-dimensionalization and expansion procedure is given at the end of § 2, after the basic

https://doi.org/10.1017/jfm.2015.503 Published online by Cambridge University Press

model has been stated. The boundary layer model is then solved numerically in § 7, with particular focus on finding margin migration velocities as a function of forcing parameters imposed by ice stream and ice ridge for the case of a widening ice stream. We summarize our findings in § 8.

2. The model

We model the ice sheet as a three-dimensional Stokes flow satisfying

$$\frac{\partial \tau_{ij}}{\partial x_j} - \frac{\partial p}{\partial z_j} + \rho g_i = 0, \tag{2.1}$$

where τ_{ij} is the deviatoric stress tensor, p is pressure, ρ is the density of ice and $\boldsymbol{g} = (0, 0, -g)$ is acceleration due to gravity. We assume a Cartesian coordinate system with the z-axis oriented vertically upwards, and use $(x_1, x_2, x_3) = (x, y, z)$ as well as the summation convention. Deviatoric stresses are related to strain rates D_{ij} through Glen's shear-thinning power-law rheology (Paterson 1994)

$$D_{ij} = A\tau^{n-1}\tau_{ij}, \tag{2.2}$$

with A and $n \geqslant 1$ assumed to be constant for simplicity; in a more sophisticated model, A would be treated as a function of temperature. Also, τ is the second invariant of the stress tensor, $\tau^2 = \tau_{ij}\tau_{ij}/2$, and strain rates are defined in terms of the velocity vector $\boldsymbol{u} = (u_1, u_2, u_3) = (u, v, w)$ through

$$D_{ij} = \frac{1}{2}\left(\frac{\partial u_i}{\partial x_j} + \frac{\partial u_j}{\partial x_i}\right). \tag{2.3}$$

Mass conservation requires

$$\nabla \cdot \boldsymbol{u} = 0. \tag{2.4}$$

The upper surface at $z = s(x, y, t)$ is assumed to be stress free,

$$\tau_{ij}n_j - pn_i = 0, \tag{2.5}$$

where $\boldsymbol{n}$ is the normal vector

$$\boldsymbol{n} = \left(-\frac{\partial s}{\partial x}, -\frac{\partial s}{\partial y}, 1\right) \Big/ \sqrt{1 + \left(\frac{\partial s}{\partial x}\right)^2 + \left(\frac{\partial s}{\partial y}\right)^2}. \tag{2.6}$$

The surface also satisfies the kinematic boundary condition

$$\frac{\partial s}{\partial t} + u\frac{\partial s}{\partial x} + v\frac{\partial s}{\partial y} = w + a, \tag{2.7}$$

where a is the rate of mass gain (through snowfall); if negative, a signifies a net rate of mass loss through melting or sublimation.

The ice sheet rests on a rigid bed, which for simplicity we assume to be flat and located at $z = 0$. Key to our model is that we differentiate between parts of the bed that are unfrozen and permit fast sliding, and parts that are frozen and do not permit sliding. We identify the former as ice streams, and the latter as the ice ridges that separate ice streams. To keep things simple, we assume a domain that is periodic in the y-direction with sides at $y = \pm W$, and has length L along the x-axis, where the

https://doi.org/10.1017/jfm.2015.503 Published online by Cambridge University Press

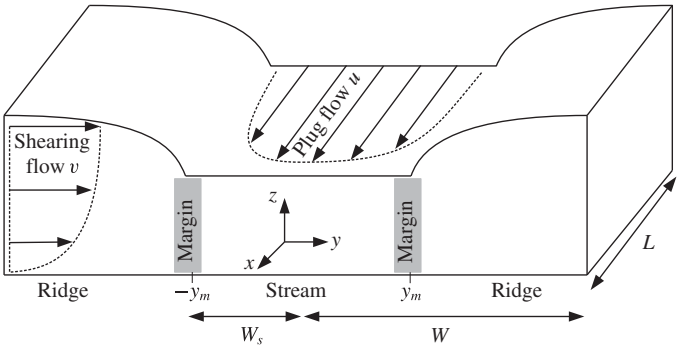


FIGURE 1. Geometry of the problem. We consider an ice stream whose principal direction of flow is along the x-axis. The y-direction is transverse to the flow, z points vertically upwards. At its sides, the ice stream is bordered by slowly moving ice or 'ice ridges'. The transition between ice stream and ice ridge is referred to here as the ice stream margin. It is located at $y = \pm y_m$. The ice ridges are symmetrical about $y = \pm W$.

latter is aligned with the main flow direction of the ice stream, see figure 1. Let a single ice stream occupy the region $-y_m < y < y_m$, where $y_m(x, t)$ signifies the location of the ice stream margin. We assume that the latter can evolve in time: in fact, one of our main objectives is to improve on the model for the migration of ice stream margins developed in Schoof (2012). Ice ridges occupy the remainder of the domain, where $y_m < |y| < W$. To simplify matters further, we assume symmetry about $y = 0$.

Different boundary conditions apply under the ice stream and ice ridge. At the base of the ice stream, $|y| < y_m$, $z = 0$, we assume that the direction of the tangential component of traction is given by the sliding velocity and its magnitude by a friction law,

$$\tau_{jk}\hat{n}_k(\delta_{ij} - \hat{n}_i\hat{n}_j) = \tau_b \frac{u_i}{|\boldsymbol{u}|}, \tag{2.8a}$$

$$\tau_b = \tau_b(|\boldsymbol{u}|, N), \tag{2.8b}$$

where we assume $\boldsymbol{u} \neq \boldsymbol{0}$. Here, τ_b is the magnitude of basal friction, which we assume to be given through a friction law as a function of the sliding speed $|\boldsymbol{u}|$ and possibly of other variables such as effective pressure N (this being the difference between normal stress at the bed and water pressure in the bed, see e.g. Iken & Bindschadler 1986; Fowler 1987; Engelhardt & Kamb 1997; Iverson *et al.* 1999; Kamb 2001; Schoof 2005; Gagliardini *et al.* 2007). We do not specify a particular friction law at this point, but will instead later assume that τ_b remains low enough everywhere in the ice stream to facilitate rapid sliding. Finally, $\hat{\boldsymbol{n}}$ is the inward- (or upward-) pointing unit vector, $\hat{\boldsymbol{n}} = (0, 0, 1)$ for a flat bed. In addition, we assume no basal melting or accretion of ice, so that

$$\boldsymbol{u} \cdot \hat{\boldsymbol{n}} = 0. \tag{2.9}$$

At the base of the ice ridges we assume that there is no slip,

$$\boldsymbol{u} = \boldsymbol{0} \tag{2.10}$$

for $|y| > y_m$, $z = 0$. The abrupt switch from slip to no slip is known to lead to stress singularities (Hutter & Olunloyo 1980; Barcilon & MacAyeal 1993; Schoof 2004;

https://doi.org/10.1017/jfm.2015.503 Published online by Cambridge University Press

Moore, Iverson & Cohen 2010), which can be alleviated if there is residual sliding even where the bed is frozen (Fowler 1986; Cuffey *et al.* 1999; Schoof 2004). In keeping with making the simplest possible assumption, we retain the no-slip boundary condition (2.10) and address the regularizing effect of having limited slip at the bed of the ice ridge in a separate paper (Haseloff, Schoof & Gagliardini, in preparation).

We associate the switch from no slip to slip with temperature at the bed attaining the melting point. Consequently we need to solve for temperature T. Within the ice, $0 < z < s(x, y, t)$, heat is both advected and conducted, and produced through strain heating, while in the bed, $z < 0$, there is only conduction:

$$\rho\, c \left(\frac{\partial T}{\partial t} + \boldsymbol{u} \cdot \boldsymbol{\nabla} T \right) - \boldsymbol{\nabla} \cdot (k \boldsymbol{\nabla} T) = D_{ij} \tau_{ij} \quad \text{for } 0 < z < s(x, y, t), \tag{2.11a}$$

$$\rho_{bed}\, c_{bed} \frac{\partial T}{\partial t} - \boldsymbol{\nabla} \cdot (k_{bed} \boldsymbol{\nabla} T) = 0 \quad \text{for } z < 0. \tag{2.11b}$$

Here, c and c_{bed} are the specific heat capacities of ice and bed, respectively, ρ_{bed} is the density of the bed, and k and k_{bed} are the thermal conductivities of ice and bed.

We assume a constant temperature T_0 at the surface $z = s(x, y, t)$ and a constant incoming geothermal heat flux q_{geo} at large depths below the bed:

$$T = T_0 \quad \text{at } z = s(x, y, t), \tag{2.12a}$$

$$-k_{bed} \frac{\partial T}{\partial z} \to q_{geo} \quad \text{as } z \to -\infty. \tag{2.12b}$$

At the ice–bed interface, we again have to distinguish between ice stream and ridge. At the base of the ice stream, the bed is at the melting point, while at the base of the ice ridge, temperature is below the melting point and the normal component of the heat flux is continuous:

$$T = T_m \quad \text{for } |y| < y_m, \quad z = 0, \tag{2.13a}$$

$$T < T_m \quad \text{and} \quad -k \left. \frac{\partial T}{\partial z} \right|^{+} + k_{bed} \left. \frac{\partial T}{\partial z} \right|^{-} = 0 \quad \text{for } |y| > y_m, \quad z = 0. \tag{2.13b}$$

Below, we non-dimensionalize the model in three different ways, appropriate to three distinct regions: the rapidly sliding ice stream, the slowly flowing ice ridge, and a narrow boundary layer that couples those regions together. This is in each case the basis for a simplified, leading-order model for ice flow and heat transport in each region. In the ridge and stream regions, these leading-order models are standard thin-film models, while in the boundary layer, we are primarily able to simplify the shape of the domain and boundary conditions, and to decouple partially the description of axial flow parallel to the ice stream in the boundary layer from transverse flow of ice across the boundary layer.

The scale applied to each variable is indicated by a square bracket with a subscript denoting the region under consideration. For example, $[u]_r$ is the scale for the velocity component u in the ice ridge, which we then non-dimensionalize as $u = [u]_r u_r$ unless otherwise indicated, so that u_r is then a dimensionless velocity in the ice ridge. Similarly, $[u]_s$ is the scale for the same velocity component in the ice stream, with u_s the corresponding dimensionless velocity in the ice stream, while $[u]_{BL}$ is the scale in the boundary layer. To reduce the number of subscripts that ultimately appear, we use capital letters to denote dimensionless variables in the boundary layer, so $u = [u]_{BL} U$

https://doi.org/10.1017/jfm.2015.503 Published online by Cambridge University Press

Description	Symbol	Value	Units
Fluidity parameter	A	1×10^{-16}	$\mathrm{kPa}^{-3}\ \mathrm{s}^{-1}$
Rheological exponent	n	3	
Specific heat capacity	c	2	$\mathrm{kJ\ kg}^{-1}\ \mathrm{K}^{-1}$
Acceleration due to gravity	g	9.81	$\mathrm{m\ s}^{-2}$
Thermal conductivity	k	2.3	$\mathrm{W\ m}^{-1}\ \mathrm{K}^{-1}$
Geothermal heat flux	q_{geo}	4×10^{-2}	$\mathrm{W\ m}^{-2}$
Density of ice	ρ	920	$\mathrm{kg\ m}^{-3}$
Accumulation rate	a	0.3	$\mathrm{m\ year}^{-1}$
Ice stream length	L	1000	km
Surface temperature	T_0	250	K
Melting point	T_m	270	K
Ice stream half-width	W_s	25	km
Domain half-width	W	50	km

TABLE 1. Parameter values and characteristic scales.

in the boundary layer. Where we deviate from this convention, we explicitly specify the definition of the relevant dimensionless variable. Typical values of parameters and the characteristic scales which we use to guide our analysis are given in table 1.

Our approach is somewhat non-standard for what is ultimately an exercise in matched asymptotic expansions: rather than non-dimensionalizing the model once for one of the three regions identified and then rescaling the dimensionless model for the other two, we develop explicit scales for all variables in all three regions. This requires somewhat careful bookkeeping when we come to match asymptotically, but we have found our approach easier to motivate physically, and less confusing to present.

In particular, we find that a number of small parameters describing various geometrical aspect ratios arise naturally in the non-dimensionalization of ice ridge and ice stream flow. These are denoted by ϵ_s, ϵ_r for the width-to-length ratios of stream and ridge, and δ_s, δ_r for the respective thickness-to-width ratios. All are assumed to be small, which allows us to develop thin-film models for ice ridges and ice streams. However, although they appear naturally when non-dimensionalizing the Stokes equations for ice ridge and ice stream, they are not all mutually independent, which is where the careful bookkeeping becomes relevant (see table 2 for a summary). In addition, we obtain a fifth aspect ratio λ (also not independent of the remaining aspect ratios) that gives a measure of ice surface slope in the boundary layer. Our leading-order model for the boundary layer is based on expanding in this additional aspect ratio λ, which must also be small.

3. Ice stream

The fast surface velocities of ice streams that are not confined to deep bedrock troughs (which we have already excluded by assuming a flat bed) can generally only be explained by rapid sliding at the bed, with comparatively little shearing across the thickness of the ice (e.g. Engelhardt & Kamb 1998). Such ice streams flow as plug flows, and appropriate leading-order models of ice streams as rapidly sliding thin-film Stokes flows have been derived by e.g. Muszynski & Birchfield (1987) and MacAyeal (1989). We follow these earlier authors, but additionally take the lateral confinement of the ice stream and its coupling with the surrounding ice ridge into account.

https://doi.org/10.1017/jfm.2015.503 Published online by Cambridge University Press

Definition	Definition
$\epsilon_s = W_s/L$	$\delta_r = [z]_r/W = \epsilon_s^{(2n+3)/(2n+2)}\epsilon_r^{-(n+2)/(2n+2)}\delta_s^{1/2}$
$\epsilon_r = W/L$	$\lambda = \begin{cases} \dfrac{[\tau_{yz}]_{BL}}{[\tau_{xy}]_{BL}} = \epsilon_s^2\delta_s^{-1} & \text{for } \dfrac{\epsilon_s}{\delta_s} \lesssim 1 \\ \dfrac{[\tau_{xy}]_{BL}}{[\tau_{yz}]_{BL}} = \epsilon_s^{1+(1/n)}\delta_s^{-(1/n)} & \text{for } \dfrac{\epsilon_s}{\delta_s} \gg 1 \end{cases}$
$\delta_s = [z]_s/W_s = \left(\dfrac{[a]}{A(\rho g)^n L^{n+1}}\dfrac{\epsilon_r}{\epsilon_s^{2n+3}}\right)^{1/(n+1)}$	$\gamma = [z]_s/[z]_r = \epsilon_s^{-(1/(2n+2))}\epsilon_r^{-(n/(2n+2))}\delta_s^{1/2}$

TABLE 2. Aspect ratios used in the matched asymptotic expansions. The three ratios on the left, ϵ_s, ϵ_r and δ_s, can be chosen independently, in which case the remaining three ratios δ_r, λ and γ can be expressed as indicated. Our asymptotic expansions assume not only that $\epsilon_s \ll 1$, $\epsilon_r \ll 1$, $\delta_s \ll 1$ but also that $\delta_r \ll 1$, $\lambda \ll 1$ as well as $\gamma \lesssim 1$. This imposes additional constraints on the ratios ϵ_s, ϵ_r and δ_s in the form $\delta_s \ll \epsilon_s^{-(2n+3)/(n+1)}\epsilon_r^{(n+2)/(n+1)}$, $\delta_s \lesssim \epsilon_s^{1/(n+1)}\epsilon_r^{n/(n+1)}$, and either $\epsilon_s \lesssim \delta_s$ or $\epsilon_s^{1+1/n} \ll \delta_s \ll \epsilon_s$. It is easy to see that such a parameter regime is possible.

Our key assumptions are therefore that the ice stream has not only a small thickness-to-width (or vertical) aspect ratio, but also a small width-to-length (or plan view) aspect ratio, as is typically the case of a narrow and long ice stream. Later, we add four further assumptions: that the ice ridge likewise has small vertical and plan view aspect ratios, that the surface slope in the ice ridge is angled primarily towards the ice stream, and that the ratio of deviatoric to hydrostatic stresses in the boundary layer is small. The latter ensures that surface slopes remain small not only in the ridge and stream, but also in the shear margin. All of these basic assumptions are satisfied in practice by ice streams in West Antarctica.

We will show as we develop our leading-order model that these assumptions can be cast as constraints on just three independent dimensionless groups. The first is the plan aspect ratio of the ice stream, which we assume to be known (for instance, from the initial plan shape of the ice stream). If the stream has length $[x]_s = L$ and half-width $[y]_s = W_s$, we assume that the plan view aspect ratio

$$\epsilon_s = \frac{W_s}{L} \tag{3.1}$$

is small. (Recall that the subscripted notation used here for scales and later for dimensionless variables is summarized at the end of § 2 above.) With $L \approx 1000$ km and $W_s \approx 25$ km, we have $\epsilon_s \approx 0.025$. An analogous (but independent) plan aspect ratio for the domain as a whole can be defined as

$$\epsilon_r = \frac{W}{L}. \tag{3.2}$$

With a spacing between neighbouring ice streams (and hence a domain width $2W$) of 100 km, $\epsilon_r \approx 0.05$, and we will treat ϵ_r as small; naturally, as the ice stream cannot be wider than the domain, we always have $\epsilon_s < \epsilon_r$.

The third independent dimensionless group is the vertical aspect ratio of the ice stream, which requires us to define a thickness scale $[z]_s$. In addition to scales L and W_s, we assume that an accumulation rate scale $[a]$ is given, as are the material

https://doi.org/10.1017/jfm.2015.503 Published online by Cambridge University Press

parameters A, n, ρ and acceleration due to gravity g. As we will see, it is possible to derive from these the appropriate scales for velocities, stresses and ice thickness.

We assume that pressure scales with its hydrostatic magnitude $[p]_s = \rho g[z]_s$. A balance between the longitudinal pressure gradient and lateral as well as vertical shear stresses yields $[\tau_{xy}]_s/W_s = [\tau_{xz}]_s/[z]_s = [p]_s/L$, while balancing terms in the velocity divergence gives $[u]_s/L = [v]_s/W_s = [w]_s/[z]_s$. Assuming flow dominated by lateral shearing, we put $[u]_s/W_s = A[\tau_{xy}]_s^n$, while the normal stress components scale as $A[\tau_{xy}]^{n-1}[\tau_{xx}]_s = [u]_s/L$, $A[\tau_{xy}]_s^{n-1}[\tau_{yy}]_s = [v]_s/W_s$ and $A[\tau_{xy}]_s^{n-1}[\tau_{zz}]_s = [w]_s/[z]_s$. The vertical shear stress associated with transverse flow balances extensional stresses in that region, leading to $[\tau_{yz}] = [z]_s[\tau_{yy}]_s/W_s$. The basal shear stress τ_b is assumed to scale as the vertical shear stress, $[\tau_b]_s = [\tau_{xz}]_s$. Ice discharge through the width of the ice stream scales as $[u]_s[z]_s W_s$, which we assume to balance net accumulation over the domain, $[u]_s[z]_s W_s = [a]WL$. Lastly, as a temperature scale, we naturally choose $[T] = T_m - T_0$, and pick the advective time scale $[t] = L/[u]_s$. We omit the subscript s on the latter two as the same scales for temperature and time apply to all three regions.

From the balances above, we can compute the scale for ice thickness in the ice stream as

$$[z]_s = \frac{L}{W_s}\left(\frac{[a]}{A(\rho g)^n}\frac{W}{W_s}\right)^{1/(n+1)} \tag{3.3}$$

from which we can define

$$\delta_s = \frac{[z]_s}{W_s}, \tag{3.4}$$

where δ_s is independent of ϵ_s and ϵ_r; $[z]_s$ defined in this way is the scale for ice thickness that emerges from requiring that discharge in the ice stream balances accumulation over the domain. If the assumptions stated in the previous paragraph about how different scales balance are correct, then the scale height $[z]_s$ should be comparable with the measured thickness of real ice streams; this is indeed the case. With the typical parameter values given in table 1, we find $[z]_s \approx 900$ m and $\delta_s \approx 0.04$. It is the fact that δ_s is small that allows us to develop a thin-film model for the ice stream.

The remaining scales for the ice stream flow problem can be expressed as

$$[x]_s = L, \quad [y]_s = W_s, \quad [s]_s = [z]_s, \tag{3.5a–c}$$

$$[u]_s = \left(\frac{\epsilon_s}{\epsilon_r}A\,(\rho g[a])^n\right)^{1/(n+1)} W, \quad [v]_s = \epsilon_s[u]_s, \quad [w]_s = \epsilon_s\delta_s[u]_s, \tag{3.5d–f}$$

$$[p]_s = \rho g[z]_s, \quad [\tau]_s = [\tau_{xy}]_s = \epsilon_s[p]_s, \quad [\tau_{xx}]_s = [\tau_{yy}]_s = [\tau_{zz}]_s = \epsilon_s^2[p]_s, \tag{3.5g–i}$$

$$[\tau_{xz}]_s = [\tau_b]_s = \delta_s\epsilon_s[p]_s, \quad [\tau_{yz}]_s = \delta_s\epsilon_s^2[p]_s, \tag{3.5j,k}$$

$$[t] = \frac{\epsilon_s[z]_s}{\epsilon_r[a]}, \quad [T] = T_m - T_0. \tag{3.5l,m}$$

In addition to the aspect ratios ϵ_s, ϵ_r and δ_s, we obtain the following independent dimensionless groups that only appear in the heat flow component of our model:

$$Pe_s = \rho c[a]W\delta_s/k, \quad \alpha_s = 2\epsilon_s\epsilon_r\delta_s^2\rho g[a]L^2/(k[T]), \quad \nu_s = [z]_s q_{geo}/(k[T]), \tag{3.6a–c}$$

$$\Gamma = \frac{\rho_{bed}}{\rho}\frac{c_{bed}}{c}, \quad \kappa = \frac{k_{bed}}{k}. \tag{3.6d,e}$$

https://doi.org/10.1017/jfm.2015.503 Published online by Cambridge University Press

Definition	Definition
$\alpha_s = 2\dfrac{A[\tau_{xy}]_s^{n+1}[z]_s^2}{k[T]} = 2\dfrac{\rho g[a]L^2}{k[T]}\epsilon_s\epsilon_r\delta_s^2$	$\alpha_r = 2\dfrac{A[\tau_{yz}]_r^{n+1}[z]_r^2}{k[T]} = \epsilon_s^{(n+2)/(n+1)}\epsilon_r^{-1/(n+1)}\delta_s^{-1}\alpha_s$
$\nu_s = \dfrac{q_{geo}[z]_s}{k[T]} = \dfrac{q_{geo}L}{k[T]}\epsilon_s\delta_s$	$\alpha_{BL} = 2\dfrac{A[\tau]_{BL}^{n+1}[z]_{BL}^2}{k[T]} = \begin{cases}\alpha_s & \text{for } \dfrac{\epsilon_s}{\delta_s} \lesssim 1 \\ \epsilon_s^{1+1/n}\delta_s^{-1-1/n}\alpha_s & \text{for } \dfrac{\epsilon_s}{\delta_s} \gg 1\end{cases}$
$Pe_s = \dfrac{[a]\rho cL}{k}\epsilon_r\delta_s$	$\nu_r = \dfrac{q_{geo}[z]_r}{k[T]} = \epsilon_s^{1/(2n+2)}\epsilon_r^{n/(2n+2)}\delta_s^{-1/2}\nu_s$
$\Gamma = \dfrac{\rho_{bed}}{\rho}\dfrac{c_{bed}}{c}$	$Pe_r = \dfrac{\rho c[a][z]_r}{k} = \delta_r\delta_s^{-1}Pe_s = \epsilon_s^{(2n+3)/(2n+2)}\epsilon_r^{-(n+2)/(2n+2)}\delta_s^{-1/2}Pe_s$
$\kappa = \dfrac{k_{bed}}{k}$	$Pe_{BL} = \dfrac{\rho c[a]W}{k} = \delta_s^{-1}Pe_s$

TABLE 3. Dimensionless groups. α_s, Pe_s, ν_s, Γ and κ are independent dimensionless groups in the model along with ϵ_s, ϵ_r and δ_s. The remaining model parameters can be expressed through these, as indicated.

These are, respectively, a Péclet number for the ice stream, a dimensionless shear heating rate, a dimensionless geothermal heat flux, and two purely material ratios of heat capacities and thermal conductivities that we will treat as being $O(1)$ constants. With the parameter values in table 1, we get $Pe_s \approx 14$, $\alpha_s \approx 6$ and $\nu_s \approx 0.8$. Note that a summary of all aspect ratios used in this paper may be found in table 2, while all other dimensionless groups used are listed in table 3. In what follows, we assume that the three aspect ratios ϵ_s, ϵ_r and δ_s are all small, while we treat the thermal parameters Pe_s, α_s and ν_s as potentially $O(1)$ for now.

3.1. *Leading-order ice stream model*

We non-dimensionalize as $u = [u]_s u_s$, $v = [v]_s v_s$, etc. and put $y_m = [y]_s y_M$, $T = T_m + [T]T_s$. Note that we use a single dimensionless time variable to describe the evolution of the entire ice mass, and continue to use the same symbol t to denote it as we did for its dimensional counterpart, omitting the subscript s.

At lowest order, omitting terms of $O(\epsilon_s^2)$, the momentum balance equation (2.1) is

$$\frac{\partial \tau_{xy,s}}{\partial y_s} + \frac{\partial \tau_{xz,s}}{\partial z_s} - \frac{\partial p_s}{\partial x_s} = 0, \tag{3.7a}$$

$$\frac{\partial p_s}{\partial y_s} = 0, \tag{3.7b}$$

$$\frac{\partial p_s}{\partial z_s} = -1. \tag{3.7c}$$

The second stress invariant only depends on the lateral shear stress $\tau_{xy,s}$:

$$\tau_s = |\tau_{xy,s}|, \tag{3.8}$$

https://doi.org/10.1017/jfm.2015.503 Published online by Cambridge University Press

where we have again omitted terms of $O(\delta_s^2)$ and $O(\epsilon_s^2)$. The constitutive relations also simplify significantly:

$$\frac{1}{2}\frac{\partial u_s}{\partial y_s} = |\tau_{xy,s}|^{n-1}\tau_{xy,s}, \quad \frac{\partial u_s}{\partial x_s} = |\tau_{xy,s}|^{n-1}\tau_{xx,s}, \tag{3.9a,b}$$

$$\frac{\partial u_s}{\partial z_s} = 0, \quad \frac{\partial v_s}{\partial y_s} = |\tau_{xy,s}|^{n-1}\tau_{yy,s}, \tag{3.9c,d}$$

$$\frac{\partial v_s}{\partial z_s} = 0, \quad \frac{\partial w_s}{\partial z_s} = |\tau_{xy,s}|^{n-1}\tau_{zz,s}. \tag{3.9e,f}$$

As in the ice stream model derived by MacAyeal (1989), the vertical gradients of both horizontal velocity components are negligible. However, our model deviates from MacAyeal's original model in that we only retain gradients of along-stream velocity u_s with respect to the cross-stream coordinate y_s in the computation of leading-order stresses ($\tau_{zz,s}$ turns out to be a higher-order correction to (3.7*c*)). This is a consequence of the small plan aspect ratio $\epsilon_s = W_s/L$, which makes our leading-order model akin to a thin-film flow version of flow in a channel or pipe (MacAyeal's model by contrast would put $\epsilon_s = 1$). The equation of mass conservation keeps its form in the scaled variables

$$\frac{\partial u_s}{\partial x_s} + \frac{\partial v_s}{\partial y_s} + \frac{\partial w_s}{\partial z_s} = 0. \tag{3.10}$$

The leading-order surface boundary conditions at $z_s = s_s(x_s, y_s, t)$ are (omitting terms of $O(\epsilon_s^2)$)

$$\frac{\partial s_s}{\partial y_s} = 0, \quad p_s = 0, \quad \tau_{xz,s} = 0. \tag{3.11a–c}$$

The first of these equalities shows that the surface is flat in the across-stream direction. The evolution of the surface is determined by

$$w_s + \frac{\epsilon_s}{\epsilon_r}a = u_s\frac{\partial s_s}{\partial x_s} + v_s\frac{\partial s_s}{\partial y_s} + \frac{\partial s_s}{\partial t} = u_s\frac{\partial s_s}{\partial x_s} + \frac{\partial s_s}{\partial t} \tag{3.11d}$$

on account of (3.11*a*). The scaled boundary conditions at the base $z_s = 0$ are

$$\tau_{xz,s} = \tau_{b,s}\frac{u_s}{|u_s|}, \quad \tau_{yz,s} = \tau_{b,s}\frac{v_s}{|u_s|}, \quad w_s = 0, \tag{3.12a–c}$$

where we have restricted ourselves to $|y_s| < y_M$.

At leading-order (again omitting terms of $O(\delta_s^2)$) the heat equation becomes

$$Pe_s\left(\frac{\partial T_s}{\partial t} + u_s\frac{\partial T_s}{\partial x_s} + v_s\frac{\partial T_s}{\partial y_s} + w_s\frac{\partial T_s}{\partial z_s}\right) - \frac{\partial^2 T_s}{\partial z_s^2} = \alpha_s|\tau_{xy,s}|^{n+1} \quad \text{for } 0 < z_s < s_s(x_s, t), \tag{3.13a}$$

$$Pe_s\Gamma\frac{\partial T_s}{\partial t} - \kappa\frac{\partial^2 T_s}{\partial z_s^2} = 0 \quad \text{for } z_s < 0. \tag{3.13b}$$

https://doi.org/10.1017/jfm.2015.503 Published online by Cambridge University Press

The scaled boundary conditions for the heat equation are

$$T_s = -1 \quad \text{at } z_s = s_s(x_s, t), \qquad T_s = 0 \quad \text{at } z_s = 0, \qquad -\kappa \frac{\partial T_s}{\partial z_s} \to \nu_s \quad \text{as } z_s \to -\infty. \tag{3.14a–c}$$

In writing down (3.13) we have again restricted ourselves to $|y_s| < y_M$.

3.2. *Integration*

We can immediately integrate (3.7*c*) using (3.11*b*) to show that $p_s = (s_s - z_s)$. From (3.9) we see that u_s depends on x_s, y_s and t only. Integrating (3.7*a*) from $z_s = 0$ to $z_s = s_s$ and using (3.11*c*) and (3.12*a*) yields the following elliptic equation for u_s (see also Raymond 1996), which is a reduced version of the more complicated, two-dimensional model in MacAyeal (1989):

$$\frac{1}{2^{1/n}} \frac{\partial}{\partial y_s} \left[s_s \left| \frac{\partial u_s}{\partial y_s} \right|^{(1-n)/n} \frac{\partial u_s}{\partial y_s} \right] - \tau_{b,s} \frac{u_s}{|u_s|} = s_s \frac{\partial s_s}{\partial x_s}, \tag{3.15}$$

where we have also used (3.11*a*) to show that s_s depends on x_s and t only. Note that, because we assume a flat bed at $z_s = 0$, s_s is both the location of the upper surface and the ice thickness.

An evolution equation of s_s can be derived by integrating (3.10) from $z_s = 0$ to $z_s = s_s$, and from $y_s = -y_M$ to $y_s = y_M$, and using (3.12*c*):

$$\int_0^{s_s} \int_{-y_M}^{y_M} \frac{\partial u_s}{\partial x_s} \, \mathrm{d}y_s \, \mathrm{d}z_s + \int_{-y_M}^{y_M} w_s|_{z_s = s_s} \, \mathrm{d}y_s + \int_0^{s_s} v_s|_{y_s = y_M} - v_s|_{y_s = -y_M} \, \mathrm{d}z_s = 0. \tag{3.16}$$

Using the fact that u_s is independent of z_s and also v_s is independent of z_s, (3.9), and using the kinematic boundary condition (3.11*d*) we can write

$$\int_{-y_M}^{y_M} s_s \frac{\partial u_s}{\partial x_s} \, \mathrm{d}y_s + \int_{-y_M}^{y_M} \left(\frac{\partial s_s}{\partial t} + u_s \frac{\partial s_s}{\partial x_s} - \frac{\epsilon_s}{\epsilon_r} a \right) \mathrm{d}y_s + 2 v_s|_{y_s = y_M} s_s = 0, \tag{3.17}$$

where we have also used that $v_s|_{y_s = y_M} = -v_s|_{y_s = -y_M}$ as we assume symmetry about $y_s = 0$. Using the fact that s_s is independent of y_s and again invoking the assumed symmetry of the ice stream, we can rewrite (3.17) as

$$\frac{\partial (2 y_M s_s)}{\partial t} + \frac{\partial Q}{\partial x_s} = \frac{\epsilon_s}{\epsilon_r} \int_{-y_M}^{y_M} a \, \mathrm{d}y + q_{in}, \tag{3.18a}$$

where

$$Q(x_s, t) = \int_{-y_M(x_s,t)}^{y_M(x_s,t)} s_s(x_s, t) u_s(x_s, y_s, t) \, \mathrm{d}y_s \tag{3.18b}$$

and

$$q_{in} = 2 s_s \left(\frac{\partial y_M}{\partial t} - v_s(x_s, y_M, t) \right) + 2 s_s u_s(x_s, y_M, t) \frac{\partial y_M}{\partial x_s}. \tag{3.18c}$$

Equation (3.15) together with (3.18*a–c*) is the leading-order model for the ice stream. To close the model, we may require additional models for any hidden degrees of freedom that may appear in the friction law for $\tau_{b,s}$, such as effective pressure at the

https://doi.org/10.1017/jfm.2015.503 Published online by Cambridge University Press

bed (e.g. Creyts & Schoof 2009; Kyrke-Smith, Katz & Fowler 2014). In addition, the necessary boundary conditions on u_s in (3.15) as well as q_{in} and any changes in margin position y_M in (3.18) represent the coupling between the ice stream and the surrounding regions of the ice sheet. Note that the ratio ϵ_s/ϵ_r appears in (3.18*a*), representing $W_s/W < 1$ (where the inequality arises because the ice stream cannot be wider than the domain itself); ϵ_s/ϵ_r is small if the ice stream width is much less than the domain width, in which case the first (surface mass balance) term on the right-hand side of (3.18*a*) becomes negligible compared with the second (lateral inflow) term. This simply means that most accumulation of mass occurs over the ice ridges, and mass is predominantly supplied to the ice stream through lateral inflow. Determining q_{in} and changes in y_M forces us to consider the flow of the ice ridges, from where the lateral inflow has to originate, and of the boundary layer separating the ridges from the stream, which holds the key to how the margin position y_m changes in time.

4. Ice ridge

We assume that the ice is frozen to the bed and that there is no slip under the ice ridges. Ice therefore moves by vertical shear alone with surface velocities that are much slower than in the adjacent ice stream. We also assume that ice is thicker in the ice ridge than in the ice stream and the resulting gradient in surface elevation leads to a gravity-driven inflow of ice into the ice stream.

By symmetry, we restrict ourselves to the ice ridge on the left (looking upstream, see figure 1), for which $-W < y < -y_m$. Consequently, we rescale the lateral coordinate as $y = [y]_r y_r - W$ with $[y]_r = W$. The length scale $[x]_r = [x]_s = L$ is the same as for the ice stream, and the relevant plan aspect ratio is $\epsilon_r = W/L$ as defined before. In order to arrive at a thin-film model, we also need to define a small vertical aspect ratio $\delta_r = [z]_r/W$, which requires us to identify a thickness scale $[z]_r$ for the ice ridge. There is no *a priori* reason why this should be the same as for the ice stream, and we go again through the same exercise of finding the relevant balance of scales for the ice ridge.

If the dominant motion in the ice ridge is through vertical shear, then vertical shear stress balances the driving pressure gradient, so $[\tau_{xz}]_r/[z]_r = [p]_r/L$ and $[\tau_{yz}]_r/[z]_r = [p]_r/W$, where $[p_r] = \rho g[z]_r$. Flow is dominantly towards the ice stream, so $[v]_r/[z]_r = A[\tau_{yz}]_r^n$ while $[u]_r/[z]_r = A[\tau_{yz}]_r^{n-1}[\tau_{xz}]_r$. Mass conservation, (2.4), suggests $[v]_r/W = [w]_r/[z]_r$ with $[w]_r = [a]$ where $[a]$ is the scale of the surface accumulation. Scales for the remaining stress components are $[u]_r/[x]_r = A[\tau_{yz}]_r^{n-1}[\tau_{xx}]_r$, $[v]_r/[y]_r = A[\tau_{yz}]_r^{n-1}[\tau_{yy}]_r$, $[w]_r/[z]_r = A[\tau_{yz}]_r^{n-1}[\tau_{zz}]_r$, and $[u]_r/[y]_r = A[\tau_{yz}]_r^{n-1}[\tau_{xy}]_r$.

The balances above define a new thickness scale through

$$[z]_r = \left(\frac{[a]W^{n+1}}{A(\rho g)^n}\right)^{1/(2n+2)}, \tag{4.1}$$

which gives us the required fourth aspect ratio $\delta_r = [z]_r/W$, which we assume to be small. Note, however, that δ_r is not independent of the previously defined parameters ϵ_s, ϵ_r, δ_s, but can be expressed as

$$\delta_r = \epsilon_s^{(2n+3)/(2n+2)}\epsilon_r^{-(n+2)/(2n+2)}\delta_s^{(1/2)}. \tag{4.2}$$

We are therefore not only assuming that ϵ_s, ϵ_r, δ_s are small, but also that

$$\epsilon_s^{(2n+3)/(n+2)}\delta_s^{(n+1)/(n+2)} \ll \epsilon_r \ll 1. \tag{4.3}$$

https://doi.org/10.1017/jfm.2015.503 Published online by Cambridge University Press

Such a parameter regime clearly exists, and applies to real ice ridges, which have low aspect ratios: with the parameter estimates in table 1 we get $\delta_r = 0.02$.

With δ_r defined, the remaining scales can now be expressed as

$$[x]_r = L, \quad [y]_r = W, \quad [u]_r = \epsilon_r (A(\rho g)^n W^{n+1} [a]^{2n+1})^{1/(2(n+1))}, \tag{4.4a–c}$$

$$[v]_r = \epsilon_r^{-1} [u]_r, \quad [w]_r = [a] = \delta_r \epsilon_r^{-1} [u]_r, \tag{4.4d,e}$$

$$p = \rho g [z]_r, \quad [\tau]_r = [\tau_{yz}]_r = \delta_r [p]_r, \quad [\tau_{xx}]_r = \epsilon_r^2 \delta_r^2 [p]_r, \tag{4.4f–h}$$

$$[\tau_{yy}]_r = [\tau_{zz}]_r = \delta_r^2 [p]_r, \quad [\tau_{xy}]_r = \epsilon_r \delta_r^2 [p]_r, \quad [\tau_{xz}]_r = \epsilon_r \delta_r [p]_r, \tag{4.4i–k}$$

while scales for time and temperature are the same as those for the ice stream.

From these scales, we can also form new versions of the Péclet number, shear heating rate and geothermal heat flux as

$$Pe_r = \rho c [a][z]_r / k, \quad \alpha_r = 2A [\tau_{yz}]_r^{n+1} [z]_r^2 / (k[T]_r), \quad \nu_r = [z]_r q_{geo} / (k[T]). \tag{4.5a–c}$$

As with δ_r, these are, however, not independent of their equivalents in the ice stream, but related to the latter through

$$Pe_r = \delta_r \delta_s^{-1} Pe_s, \quad \alpha_r = \epsilon_s^{(n+2)/(n+1)} \epsilon_r^{-1/(n+1)} \delta_s^{-1} \alpha_s, \quad \nu_r = \epsilon_s^{-1} \epsilon_r \delta_s^{-1} \delta_r \nu_s. \tag{4.6a–c}$$

Note that the ratio of the Péclet numbers in the ice ridge and ice stream equals the ratio of the vertical aspect ratios in the two regions, and the ratio of the scaled geothermal heat fluxes depends only on the ratio between the thickness scales in the two regions. With the parameter estimates in table 1 we obtain $[z]_s \approx 900$ m and $[z]_r \approx 970$ m, and therefore calculate values of Pe_r and ν_r that are similar to those in the ice stream: we get $Pe_r \approx 7$ and $\nu_r \approx 0.8$, as well as $\alpha_r \approx 4$. As before, we retain these for now as being potentially $O(1)$.

4.1. *Leading-order ice ridge model*

We put $u = [u]_r u_r$, $v = [v]_r v_r$, etc., and $T = T_m + [T] T_r$, $y = [y]_r (y_r - 1)$. With these, the stress balance at leading order is

$$\frac{\partial \tau_{xz,r}}{\partial z_r} - \frac{\partial p_r}{\partial x_r} = 0, \tag{4.7a}$$

$$\frac{\partial \tau_{yz,r}}{\partial z_r} - \frac{\partial p_r}{\partial y_r} = 0, \tag{4.7b}$$

$$-\frac{\partial p_r}{\partial z_r} = 1. \tag{4.7c}$$

Here, terms of $O(\delta_r^2)$ were omitted. At leading order, the second stress invariant is solely a function of the vertical shear stress $\tau_{yz,r}$, i.e.

$$\tau_r = |\tau_{yz,r}|, \tag{4.8}$$

so the stress components are related to the velocity gradients at leading order through

$$\frac{1}{2}\left(\frac{\partial u_r}{\partial y_r} + \frac{\partial v_r}{\partial x_r}\right) = |\tau_{yz,r}|^{n-1} \tau_{xy,r}, \quad \frac{\partial u_r}{\partial x_r} = |\tau_{yz,r}|^{n-1} \tau_{xx,r}, \tag{4.9a,b}$$

https://doi.org/10.1017/jfm.2015.503 Published online by Cambridge University Press

$$\frac{1}{2}\frac{\partial u_r}{\partial z_r} = |\tau_{yz,r}|^{n-1}\tau_{xz,r}, \qquad \frac{\partial v_r}{\partial y_r} = |\tau_{yz,r}|^{n-1}\tau_{yy,r}, \tag{4.9c,d}$$

$$\frac{1}{2}\frac{\partial v_r}{\partial z_r} = |\tau_{yz,r}|^{n-1}\tau_{yz,r}, \qquad \frac{\partial w_r}{\partial z_r} = |\tau_{yz,r}|^{n-1}\tau_{zz,r}. \tag{4.9e,f}$$

Omitting terms of $O(\epsilon_r^2)$, mass conservation becomes

$$\frac{\partial v_r}{\partial y_r} + \frac{\partial w_r}{\partial z_r} = 0. \tag{4.10}$$

The boundary conditions at the upper surface $z_r = s_r$ are

$$\tau_{xz,r} = 0, \quad \tau_{yz,r} = 0, \quad p_r = 0, \quad w_r + a = v_r\frac{\partial s_r}{\partial y_r} + \frac{\epsilon_r^2\delta_r}{\epsilon_s^2\delta_s}\frac{\partial s_r}{\partial t}. \tag{4.11a–d}$$

The boundary conditions at the base of the ice at $z_r = 0$ are

$$u_r = v_r = w_r = 0, \tag{4.12}$$

where we have restricted ourselves to the region of no slip, $y_r < 1 - (\epsilon_s/\epsilon_r)y_M$.

The rescaled heat equation at leading order (omitting terms of $O(\delta_r^2)$, $O(\epsilon_r^2)$) is

$$Pe_r\left(\frac{\epsilon_r^2\delta_r}{\epsilon_s^2\delta_s}\frac{\partial T_r}{\partial t} + v_r\frac{\partial T_r}{\partial y_r} + w_r\frac{\partial T_r}{\partial z_r}\right) - \frac{\partial^2 T_r}{\partial z_r^2} = \alpha_r|\tau_{yz,r}|^{n+1} \quad \text{for } 0 < z_r < s_r, \tag{4.13a}$$

$$Pe_r\Gamma\frac{\epsilon_r^2\delta_r}{\epsilon_s^2\delta_s}\frac{\partial T_r}{\partial t} - \kappa\frac{\partial^2 T_r}{\partial z_r^2} = 0 \quad \text{for } z_r < 0, \tag{4.13b}$$

with boundary conditions

$$T_r = -1 \quad \text{at } z_r = s_r, \tag{4.14a}$$

$$T_r < 0 \quad \text{and} \quad \left.\frac{\partial T_r}{\partial z_r}\right|^{+} - \kappa\left.\frac{\partial T_r}{\partial z_r}\right|^{-} = 0 \quad \text{at } z_r = 0, \tag{4.14b,c}$$

$$-\kappa\frac{\partial T_r}{\partial z_r} \to v_r \quad \text{as } z_r \to -\infty. \tag{4.14d}$$

4.2. *Depth integration*

The ice flow model (4.7*a*)–(4.12), is easily recognizable as a standard viscous gravity current model for flow in the y-direction, termed a 'shallow ice' model in glaciology (Fowler & Larson 1978; Morland & Johnson 1980). It can be integrated to give

$$u_r = -\frac{2s_r^{n+1}}{n+1}\left[1 - \left(1 - \frac{z_r}{s_r}\right)^{n+1}\right]\left|\frac{\partial s_r}{\partial y_r}\right|^{n-1}\frac{\partial s_r}{\partial x_r}, \tag{4.15a}$$

$$v_r = -\frac{2s_r^{n+1}}{n+1}\left[1 - \left(1 - \frac{z_r}{s_r}\right)^{n+1}\right]\left|\frac{\partial s_r}{\partial y_r}\right|^{n-1}\frac{\partial s_r}{\partial y_r}, \tag{4.15b}$$

https://doi.org/10.1017/jfm.2015.503 Published online by Cambridge University Press

from (4.7). The evolution of the ice ridge surface is governed by

$$\frac{\epsilon_r^2 \delta_r}{\epsilon_s^2 \delta_s} \frac{\partial s_r}{\partial t} + \frac{\partial q_r}{\partial y_r} = a, \tag{4.16}$$

where

$$q_r = \int_0^{s_r} v_r \, \mathrm{d}z_r = -\frac{2}{n+2} s_r^{n+2} \left| \frac{\partial s_r}{\partial y_r} \right|^{n-1} \frac{\partial s_r}{\partial y_r}. \tag{4.17}$$

Equation (4.16) together with (4.17) is a nonlinear diffusion problem for s_r which requires a boundary condition at the ice stream margin $y_r = 1 - (\epsilon_s/\epsilon_r) y_M$. This requires us to couple the ice stream problem to the ice ridge problem, which leads us to consider a boundary layer separating the two.

5. The margin boundary layer

In the last two sections we have derived equations that describe the evolution of an ice stream, (3.15) and (3.18*a–c*), and of an ice ridge adjacent to it, (4.16) and (4.17). The ice stream moves as a plug flow through a 'channel' formed by the ice ridges, where ice moves through vertical shear towards the ice stream. At present we can only speculate about the appropriate coupling between the two models. For instance, we might expect the inflow q_{in} in (3.18*c*) to be related to the ice ridge flux q_r in (4.17) at the margin. However, due to the distinct nature of the velocity fields in the stream and ridge – one is a plug flow, the other a shearing flow – coupling is not trivial and a boundary layer is required. Similar boundary layers are encountered in other settings in ice sheet dynamics, for instance around the grounding line of marine ice sheets (Chugunov & Wilchinsky 1996).

The boundary layer here is located between the ice stream and the ice ridge in the region around $y = \pm y_m(x, t)$, which we refer to as the ice stream margin. As with the ice ridge, we focus on the margin to the left of the ice stream near $y = -y_m$. Within the boundary layer a spatially rapid transition from the Poiseuille-type flow in the ice ridge to the plug flow in the ice stream has to take place. The boundary layer cannot be shallow – otherwise we would expect one kind of thin-film approximation or the other to hold – and to account for continuity of the surface with the adjacent stream, we choose the scales $[y]_{BL} = [z]_{BL} = [z]_s$. We rescale the lateral coordinate $y = [y]_{BL} Y - [y]_s y_M(x_s, t)$, so that the boundary layer coordinate is centred around the transition between a frozen bed and an unfrozen temperate bed that occurs in the left-hand margin at $y_s = -y_M$, $Y = 0$.

To account for mass flux from the ridge through the margin into the ice stream, we put $[v]_{BL}[z]_{BL} = [v]_s[z]_s = [a]W$, or $[v]_{BL} = [v]_s$, while mass balance requires $[v]_{BL} = [w]_{BL}$. The ice stream imposes a lateral shear stress on the boundary layer, which must be balanced by vertical shear stresses in the boundary layer and leads us to put $[\tau_{xz}]_{BL} = [\tau_{xy}]_{BL} = [\tau_{xy}]_s$.

Shearing due to transverse flow in the boundary layer leads to $[v]_{BL}/[z]_{BL} = A[\tau]_{BL}^{n-1}[\tau_{yz}]_{BL}$. There are now two possible cases: the second stress invariant τ in the boundary layer can be dominated either by shear stresses due to transverse flow, so that $[\tau]_{BL} = [\tau_{yz}]_{BL}$, or by lateral shear stresses, so that $[\tau]_{BL} = [\tau_{xy}]_{BL}$. In the first case, the scaled stress invariant becomes $\mathscr{T} = (\mathscr{T}_{xy}^2 + \mathscr{T}_{xz}^2 + (\epsilon_s/\delta_s)^2 \mathscr{T}_{yz}^2 + \cdots)^{1/2}$, where $\mathscr{T}_{ij}$ denotes dimensionless stress components. It is clear that this scaling is only appropriate for $\epsilon_s/\delta_s \lesssim 1$. Similarly, the second version is only appropriate

https://doi.org/10.1017/jfm.2015.503 Published online by Cambridge University Press

for $\epsilon_s/\delta_s \gtrsim 1$, but to be definite when $\epsilon_s \sim \delta_s$, we define $[\tau]_{BL} = [\tau_{yz}]_{BL}$ only when $\epsilon_s/\delta_s \gg 1$, and put $[\tau]_{BL} = [\tau_{xy}]_{BL}$ otherwise.

The scale of the downstream velocity is defined through $[u]_{BL}/[z]_{BL} = A[\tau]_{BL}^{n-1}[\tau_{xy}]_{BL}$, and the normal components of the stress are determined through $[u]_{BL}/[x]_{BL} = A[\tau]_{BL}^{n-1}[\tau_{xx}]_{BL}$, $[v]_{BL}/[y]_{BL} = A[\tau]_{BL}^{n-1}[\tau_{yy}]_{BL}$ and $[w]_{BL}/[z]_{BL} = A[\tau]_{BL}^{n-1}[\tau_{zz}]_{BL}$. We assume that the basal drag in the unfrozen part of the margin is comparable with the basal drag in the ice stream, which for instance would be appropriate if the bed of the margin was hydraulically well connected to the ice stream bed, and we therefore put $[\tau_b]_{BL} = [\tau_b]_s$.

The leading-order models for the two cases in ϵ_s/δ_s identified above (which differ in terms of which stresses dominate the stress invariant and therefore ice viscosity and heat dissipation in the boundary layer) are very similar and we can treat them both succinctly by defining a parameter λ through

$$\lambda = \begin{cases} \epsilon_s^2/\delta_s & \text{for } \dfrac{\epsilon_s}{\delta_s} \lesssim 1, \\ (\epsilon_s^{n+1}/\delta_s)^{1/n} & \text{for } \dfrac{\epsilon_s}{\delta_s} \gg 1; \end{cases} \tag{5.1}$$

λ turns out to be the ratio of deviatoric normal stresses to hydrostatic pressure in the boundary layer. We will assume below that $\lambda \ll 1$, which ensures that the surface slope in the boundary layer remains small and we can treat the boundary layer at zeroth order as occupying a fixed domain with a flat upper surface. We always have $\lambda \ll 1$ when $\epsilon_s/\delta_s \lesssim 1$, while for $\epsilon_s/\delta_s \gg 1$, we require an additional constraint

$$\epsilon_s^{n+1} \ll \delta_s \ll \epsilon_s. \tag{5.2}$$

This is in addition to the constraint $\epsilon_s^{(2n+3)/(n+2)}\delta_s^{(n+1)/(n+2)} \ll \epsilon_r \ll 1$ from (4.3). A compilation of all the constraints that we impose on the independent parameters ϵ_s, ϵ_r and δ_s is given in the caption to table 2.

From the balances identified above, the relevant scales for the boundary layer can now be expressed as

$$[x]_{BL} = L, \quad [y]_{BL} = [z]_{BL} = [z]_s \tag{5.3a,b}$$

$$[u]_{BL} = \begin{cases} \dfrac{\epsilon_r}{\epsilon_s^2}[a] & \text{for } \dfrac{\epsilon_s}{\delta_s} \lesssim 1, \\ \dfrac{\epsilon_r}{\epsilon_s^{2/n}}\left(\dfrac{[a]^{(n^2+1)/(1-n)}}{A(\rho g)^n}\dfrac{W}{W_s^{n+2}}\right)^{(1-n)/(1+n)(1/n)} = \epsilon_r\epsilon_s^{-1-1/n}\delta_s^{-1+1/n}[a] & \text{for } \dfrac{\epsilon_s}{\delta_s} \gg 1, \end{cases} \tag{5.3c}$$

$$[v]_{BL} = [w]_{BL} = \lambda\epsilon_s^{-1}[u]_{BL}, \tag{5.3d}$$

$$[p]_{BL} = \rho g[z]_{BL} = [p]_s, \quad [\tau_{xy}]_{BL} = [\tau_{xz}]_{BL} = \epsilon_s[p]_{BL}, \quad [\tau_{xx}]_{BL} = \epsilon_s^2[p]_{BL} \tag{5.3e–g}$$

$$[\tau_b]_{BL} = [\tau_b]_s = \delta_s\epsilon_s[p]_{BL}, \quad [\tau_{yy}]_{BL} = [\tau_{zz}]_{BL} = [\tau_{yz}]_{BL} = \lambda[p]_{BL} \tag{5.3h,i}$$

$$[\tau]_{BL} = \begin{cases} \epsilon_s[p]_{BL} & \text{for } \dfrac{\epsilon_s}{\delta_s} \lesssim 1, \\ \lambda[p]_{BL} & \text{for } \dfrac{\epsilon_s}{\delta_s} \gg 1, \end{cases} \tag{5.3j}$$

https://doi.org/10.1017/jfm.2015.503 Published online by Cambridge University Press

while the scales for time and temperature are again the same as those for the ice stream itself.

In addition to the parameter λ defined above, we obtain new versions of the Péclet number and dimensionless shear rate, $Pe_{BL} = \rho c[a]W/k$ and $\alpha_{BL} = 2A[\tau]_{BL}^{n+1}[z]_{BL}^2/(k[T]_{BL})$. As with Pe_r and α_r, Pe_{BL} and α_{BL} are not independent of Pe_s, α_s, ϵ_s, ϵ_r and δ_s, but can be written in the form

$$Pe_{BL} = \delta_s^{-1} Pe_s, \quad \alpha_{BL} = \begin{cases} \alpha_s & \text{for } \dfrac{\epsilon_s}{\delta_s} \lesssim 1, \\ \epsilon_s^{1+1/n} \delta_s^{-1-1/n} \alpha_s & \text{for } \dfrac{\epsilon_s}{\delta_s} \gg 1. \end{cases} \tag{5.4a,b}$$

With the typical values in table 1, we obtain $Pe_{BL} \approx 380$ and $\alpha_{BL} \approx 6$.

5.1. *Boundary layer model*

We put $u = [u]_{BL} U$, $v = [v]_{BL} V$, $w = [w]_{BL} W$, $\tau_{xy} = [\tau_{xy}]_{BL} \mathscr{T}_{xy}$, etc., and $T = T_m + [T] T_{BL}$, $y = [y]_{BL} Y - [y]_s y_M(x_s, t)$. In the dimensionless variables, we give the boundary layer equations up to the order indicated. Force balance becomes

$$\frac{\partial \mathscr{T}_{xy}}{\partial Y} + \frac{\partial \mathscr{T}_{xz}}{\partial Z} - \delta_s \frac{\partial P}{\partial X} - \frac{\partial y_M}{\partial x_s} \frac{\partial P}{\partial Y} = 0, \tag{5.5a}$$

$$\lambda \frac{\partial \mathscr{T}_{yy}}{\partial Y} + \lambda \frac{\partial \mathscr{T}_{yz}}{\partial Z} - \frac{\partial P}{\partial Y} = 0, \tag{5.5b}$$

$$\lambda \frac{\partial \mathscr{T}_{yz}}{\partial Y} + \lambda \frac{\partial \mathscr{T}_{zz}}{\partial Z} - \frac{\partial P}{\partial Z} = 1, \tag{5.5c}$$

omitting terms of $O(\epsilon_s^2)$. The stress invariant is

$$\mathscr{T} = \begin{cases} \sqrt{\mathscr{T}_{xy}^2 + \mathscr{T}_{xz}^2 + \dfrac{\epsilon_s^2}{\delta_s^2} \mathscr{T}_{yz}^2 + \dfrac{1}{2} \dfrac{\epsilon_s^2}{\delta_s^2} \mathscr{T}_{yy}^2 + \dfrac{1}{2} \dfrac{\epsilon_s^2}{\delta_s^2} \mathscr{T}_{zz}^2} & \text{for } \dfrac{\epsilon_s}{\delta_s} \lesssim 1, \\ \sqrt{\mathscr{T}_{yz}^2 + \dfrac{1}{2} \mathscr{T}_{yy}^2 + \dfrac{1}{2} \mathscr{T}_{zz}^2} & \text{for } \dfrac{\epsilon_s}{\delta_s} \gg 1. \end{cases} \tag{5.6}$$

to $O(\epsilon_s^2)$ and $O(\delta_s^{2/n}/\epsilon_s^{2/n})$, respectively, and the stress–strain relationship can be expressed in terms of $\mathscr{T}$ as

$$\frac{1}{2} \left(\frac{\partial U}{\partial Y} + \lambda \frac{\partial y_M}{\partial x_s} \frac{\partial V}{\partial Y} \right) = \mathscr{T}^{n-1} \mathscr{T}_{xy}, \quad \frac{\partial y_M}{\partial x_s} \frac{\partial U}{\partial Y} + \delta_s \frac{\partial U}{\partial X} = \mathscr{T}^{n-1} \mathscr{T}_{xx}, \tag{5.7a,b}$$

$$\frac{1}{2} \left(\frac{\partial U}{\partial Z} + \lambda \frac{\partial y_M}{\partial x_s} \frac{\partial W}{\partial Y} \right) = \mathscr{T}^{n-1} \mathscr{T}_{xz}, \quad \frac{\partial V}{\partial Y} = \mathscr{T}^{n-1} \mathscr{T}_{yy}, \tag{5.7c,d}$$

$$\frac{1}{2} \left(\frac{\partial V}{\partial Z} + \frac{\partial W}{\partial Y} \right) = \mathscr{T}^{n-1} \mathscr{T}_{yz}, \quad \frac{\partial W}{\partial Z} = \mathscr{T}^{n-1} \mathscr{T}_{zz}, \tag{5.7e,f}$$

omitting terms of $O(\epsilon_s^2)$ and $O(\delta_s \lambda)$. To an error of $O(\epsilon_s^2/\lambda)$, mass conservation can be expressed as

$$\frac{\partial V}{\partial Y} + \frac{\partial W}{\partial Z} = 0. \tag{5.8}$$

https://doi.org/10.1017/jfm.2015.503 Published online by Cambridge University Press

The missing $O(\epsilon_s^2/\lambda)$ term is $(\epsilon_s^2/\lambda)(\partial y_M/\partial x_s)(\partial U/\partial Y)$, which appears because the margin may be tilted relative to the x-axis. This term is, however, always small as we have $\epsilon_s^2/\lambda \ll 1$: for $\epsilon_s \lesssim \delta_s$, $\epsilon_s^2/\lambda = \delta_s$, while for $\epsilon_s \gg \delta_s$, we have $\epsilon_s^2/\lambda = \epsilon_s^{1-1/n}\delta_s^{1/n}$.

The boundary conditions at the upper surface at $Z = S$ are, omitting terms of $O(\epsilon_s^2\delta_s)$,

$$-\mathscr{T}_{xy}\frac{\partial S}{\partial Y} + \mathscr{T}_{xz} + \delta_s P\frac{\partial S}{\partial X} + P\frac{\partial y_M}{\partial x_s}\frac{\partial S}{\partial Y} = 0, \tag{5.9a}$$

$$-\lambda\mathscr{T}_{yy}\frac{\partial S}{\partial Y} + \lambda\mathscr{T}_{yz} + P\frac{\partial S}{\partial Y} = 0, \tag{5.9b}$$

$$-\lambda\mathscr{T}_{yz}\frac{\partial S}{\partial Y} + \lambda\mathscr{T}_{zz} - P = 0 \tag{5.9c}$$

and, omitting terms of $O(\delta_s)$ and $O(\epsilon_s^2/\lambda)$,

$$W = V\frac{\partial S}{\partial Y} + \frac{\partial y_M}{\partial t}\frac{\partial S}{\partial Y}. \tag{5.10}$$

The boundary conditions at the base of the ice at $Z = 0$ are, omitting terms of $O(\delta_s)$,

$$\mathscr{T}_{xz} = 0, \quad \mathscr{T}_{yz} = 0, \quad W = 0 \quad \text{for } Y > 0, \tag{5.11a–c}$$

$$U = V = W = 0 \quad \text{for } Y < 0. \tag{5.11d}$$

Note that the omission of an $O(\delta_s)$ friction term for $Y > 0$ is based on our assumption that basal friction near the margin remains of similar magnitude to the amount of friction inside the ice stream proper.

Finally, the heat equation in rescaled form is

$$Pe_{BL}\left(\delta_s\frac{\partial T_{BL}}{\partial t} + \frac{\partial y_M}{\partial t}\frac{\partial T_{BL}}{\partial Y} + V\frac{\partial T_{BL}}{\partial Y} + W\frac{\partial T_{BL}}{\partial Z}\right) - \left(\frac{\partial^2 T_{BL}}{\partial Y^2} + \frac{\partial^2 T_{BL}}{\partial Z^2}\right) = \alpha_{BL}\mathscr{T}^{n+1} \quad \text{for } 0 < Z < S, \tag{5.12a}$$

$$Pe_{BL}\Gamma\left(\delta_s\frac{\partial T_{BL}}{\partial t} + \frac{\partial y_M}{\partial t}\frac{\partial T_{BL}}{\partial Y}\right) - \kappa\left(\frac{\partial^2 T_{BL}}{\partial Y^2} + \frac{\partial^2 T_{BL}}{\partial Z^2}\right) = 0 \quad \text{for } Z < 0, \tag{5.12b}$$

omitting terms of $O(\epsilon_s^2/\lambda)$ and $O(\delta_s^2)$. The boundary conditions for the heat equation are

$$T_{BL} = -1 \quad \text{at } Z = S, \quad -\kappa\frac{\partial T_{BL}}{\partial Z} = \nu_s \quad \text{as } Z \to -\infty, \tag{5.13a,b}$$

$$T_{BL} < 0 \quad \text{and} \quad -\frac{\partial T_{BL}}{\partial Z}\bigg|^{+} + \kappa\left.\frac{\partial T_{BL}}{\partial Z}\right|^{-} = 0 \quad \text{for } Y < 0,\ Z = 0, \tag{5.13c,d}$$

$$T_{BL} = 0 \quad \text{for } Y > 0,\ Z = 0. \tag{5.13e}$$

https://doi.org/10.1017/jfm.2015.503 Published online by Cambridge University Press

5.2. *Series expansion*

Our primary objective is to find leading-order models for velocities U, V and W, surface elevation S and temperature T_{BL} in the boundary layer. To do so we need to develop asymptotic expansions in λ:

$$\left.\begin{gathered} P(X,Y,Z,t) = P^{(0)}(X,Y,Z,t) + \lambda P^{(1)}(X,Y,Z,t) + o(\lambda), \\ S(X,Y,t) = S^{(0)}(X,Y,t) + \lambda S^{(1)}(X,Y,t) + o(\lambda), \\ U(X,Y,Z,t) = U^{(0)}(X,Y,Z,t) + o(1), \quad V(X,Y,Z,t) = V^{(0)}(X,Y,Z,t) + o(1), \\ W(X,Y,Z,t) = W^{(0)}(X,Y,Z,t) + o(1). \end{gathered}\right\} \tag{5.14}$$

To evaluate the pressure at the surface $Z = S = S^{(0)} + \lambda S^{(1)} + \cdots$, we can write P as a Taylor expansion

$$P(X,Y,S,t) = P^{(0)}(X,Y,S^{(0)},t) + \lambda \frac{\partial P^{(0)}}{\partial Z} S^{(1)}(X,Y,t) + \lambda P^{(1)}(X,Y,S^{(0)},t) + o(\lambda). \tag{5.15}$$

We naturally continue to assume that the other aspect ratios (ϵ_s, δ_s, ϵ_r, δ_r) remain small; the $o(1)$ and $o(\lambda)$ notation above is intended to signify that the next order of approximation may be due to terms like ϵ_s, δ_s or $\lambda\epsilon_s$, $\lambda\delta_s$ etc. rather than of $O(\lambda)$ or $O(\lambda^2)$.

At zeroth order we get from (5.5*b*) and (5.5*c*)

$$-\frac{\partial P^{(0)}}{\partial Y} = 0, \quad -\frac{\partial P^{(0)}}{\partial Z} = 1, \tag{5.16a,b}$$

with boundary condition $P^{(0)} = 0$ at $Z = S^{(0)}$ from (5.9*c*). Integration of (5.16*b*) gives $P^{(0)} = S^{(0)} - Z$ and consequently (5.16*a*) requires $\partial S^{(0)}/\partial Y = 0$. The upper surface is flat at lowest order, and the ice flow domain is a parallel-sided strip.

Combining (5.5) and (5.7), the leading-order problem for the downstream flow is

$$\frac{\partial}{\partial Y}\left(\eta \frac{\partial U^{(0)}}{\partial Y}\right) + \frac{\partial}{\partial Z}\left(\eta \frac{\partial U^{(0)}}{\partial Z}\right) = 0, \tag{5.17}$$

where the viscosity η is given by

$$\eta = \frac{1}{2^{1/n}} \begin{cases} \left[\left|\dfrac{\partial U^{(0)}}{\partial Y}\right|^2 + \left|\dfrac{\partial U^{(0)}}{\partial Z}\right|^2 + \dfrac{\epsilon_s^2}{\delta_s^2}\left(\left|\dfrac{\partial V^{(0)}}{\partial Z} + \dfrac{\partial W^{(0)}}{\partial Y}\right|^2 \right.\right. \\ \qquad \left.\left. + 2\left|\dfrac{\partial V^{(0)}}{\partial Y}\right|^2 + 2\left|\dfrac{\partial W^{(0)}}{\partial Z}\right|^2\right)\right]^{(1-n)/(2n)} & \text{for } \dfrac{\epsilon_s}{\delta_s} \lesssim 1, \\ \left[\left|\dfrac{\partial V^{(0)}}{\partial Z} + \dfrac{\partial W^{(0)}}{\partial Y}\right|^2 + 2\left|\dfrac{\partial V^{(0)}}{\partial Y}\right|^2 + 2\left|\dfrac{\partial W^{(0)}}{\partial Z}\right|^2\right]^{(1-n)/(2n)} & \text{for } \dfrac{\epsilon_s}{\delta_s} \gg 1. \end{cases} \tag{5.18}$$

https://doi.org/10.1017/jfm.2015.503 Published online by Cambridge University Press

Boundary conditions at the ice surface $Z = S^{(0)}(X, t)$ and base $Z = 0$ are

$$\eta \frac{\partial U^{(0)}}{\partial Z} = 0 \quad \text{at } Z = S^{(0)}, \tag{5.19a}$$

$$\eta \frac{\partial U^{(0)}}{\partial Z} = 0 \quad \text{at } Z = 0, \quad Y > 0, \tag{5.19b}$$

$$U^{(0)} = 0 \quad \text{at } Z = 0, \quad Y < 0. \tag{5.19c}$$

The transverse velocity $(V^{(0)}, W^{(0)})$ is the solution of

$$\frac{\partial}{\partial Y}\left(2\eta \frac{\partial V^{(0)}}{\partial Y}\right) + \frac{\partial}{\partial Z}\left[\eta\left(\frac{\partial V^{(0)}}{\partial Z} + \frac{\partial W^{(0)}}{\partial Y}\right)\right] - \frac{\partial P^{(1)}}{\partial Y} = 0, \tag{5.20a}$$

$$\frac{\partial}{\partial Y}\left[\eta\left(\frac{\partial V^{(0)}}{\partial Z} + \frac{\partial W^{(0)}}{\partial Y}\right)\right] + \frac{\partial}{\partial Z}\left(2\eta \frac{\partial V^{(0)}}{\partial Y}\right) - \frac{\partial P^{(1)}}{\partial Z} = 0, \tag{5.20b}$$

$$\frac{\partial V^{(0)}}{\partial Y} + \frac{\partial W^{(0)}}{\partial Z} = 0, \tag{5.20c}$$

with boundary conditions

$$W^{(0)} = \eta\left(\frac{\partial V^{(0)}}{\partial Z} + \frac{\partial W^{(0)}}{\partial Y}\right) = 0, \quad 2\eta \frac{\partial W^{(0)}}{\partial Z} - P^{(1)} + S^{(1)} = 0 \quad \text{at } Z = S^{(0)} \tag{5.21a,b}$$

at the ice surface. Boundary conditions at the base are

$$\eta\left(\frac{\partial V^{(0)}}{\partial Z} + \frac{\partial W^{(0)}}{\partial Y}\right) = W^{(0)} = 0 \quad \text{for } Y > 0, \quad Z = 0, \tag{5.22a}$$

$$V^{(0)} = W^{(0)} = 0 \quad \text{for } Y < 0, \quad Z = 0. \tag{5.22b}$$

For $n = 1$, the transverse flow model (5.20)–(5.22) is almost identical to the model for ice flowing across a no-slip-to-free-slip transition boundary in Barcilon & MacAyeal (1993), although the latter was originally conceived for a different geometry than ours and their far-field boundary conditions are not entirely identical to the ones we will derive below. The axial flow model (5.17)–(5.19) for $n = 1$ is, furthermore, the same as that in Schoof (2012).

We leave the temperature problem (in which λ does not appear) unchanged from (5.12) and (5.13) for now, except that we use the leading-order versions of the velocity components and treat the upper surface as flat. Our estimates suggest that Péclet numbers P_{BL} should be large, which can be dealt with in terms of an additional thermal boundary layer structure that we explore in a separate paper (Haseloff *et al.*, in preparation).

6. Matching

The boundary layer solutions have to match the solutions in the outer regions, the ice stream and ridge. Even though we have motivated all our scales physically, the spatial coordinates and dependent variables used to describe the stream, ridge and boundary layer can be related purely through rescalings using the independent aspect ratios ϵ_s, ϵ_r, δ_s, and the derived dimensionless groups δ_r and λ defined in

https://doi.org/10.1017/jfm.2015.503 Published online by Cambridge University Press

terms of ϵ_s, ϵ_r and δ_s in (4.2) and (5.1), respectively. We list these rescalings here for completeness:

$$x_s = x_r = X, \quad y_s = \frac{\epsilon_r}{\epsilon_s}(y_r - 1) = \delta_s Y - y_M(x_s, t), \quad z_s = \frac{\epsilon_s \delta_s}{\epsilon_r \delta_r} z_r = Z, \tag{6.1a–c}$$

$$u_s = \frac{\epsilon_s^2 \delta_s}{\delta_r} u_r = \frac{\epsilon_s^2}{\lambda} U, \quad v_s = \frac{\epsilon_s \delta_s}{\epsilon_r \delta_r} v_r = V, \quad w_s = \frac{\epsilon_s}{\epsilon_r} w_r = \frac{1}{\delta_s} W, \tag{6.1d–f}$$

$$p_s = \frac{\epsilon_r \delta_r}{\epsilon_s \delta_s} p_r = P, \quad \tau_s = \frac{\epsilon_r \delta_r^2}{\epsilon_s^2 \delta_s} \tau_r = \begin{cases} \mathscr{T} & \text{for } \dfrac{\epsilon_s}{\delta_s} \lesssim 1, \\ \left(\dfrac{\epsilon_s}{\delta_s}\right)^{1/n} \mathscr{T} & \text{for } \dfrac{\epsilon_s}{\delta_s} \gg 1, \end{cases} \tag{6.1g,h}$$

$$\tau_{xx,s} = \frac{\epsilon_r^3 \delta_r^3}{\epsilon_s^3 \delta_s} \tau_{xx,r} = \mathscr{T}_{xx}, \quad \tau_{yy,s} = \frac{\epsilon_r \delta_r^3}{\epsilon_s^3 \delta_s} \tau_{yy,r} = \frac{\lambda}{\epsilon_s^2} \mathscr{T}_{yy}, \tag{6.1i,j}$$

$$\tau_{zz,s} = \frac{\epsilon_r \delta_r^3}{\epsilon_s^3 \delta_s} \tau_{zz,r} = \frac{\lambda}{\epsilon_s^2} \mathscr{T}_{zz}, \quad \tau_{xy,s} = \frac{\epsilon_r^2 \delta_r^3}{\epsilon_s^2 \delta_s} \tau_{xy,r} = \mathscr{T}_{xy}, \tag{6.1k,l}$$

$$\tau_{xz,s} = \frac{\epsilon_r^2 \delta_r^2}{\epsilon_s^2 \delta_s^2} \tau_{xz,r} = \frac{1}{\delta_s} \mathscr{T}_{xz}, \quad \tau_{yz,s} = \frac{\epsilon_r \delta_r^2}{\epsilon_s^3 \delta_s^2} \tau_{yz,r} = \frac{\lambda}{\epsilon_s^2 \delta_s} \mathscr{T}_{yz}, \tag{6.1m,n}$$

$$T_s = T_r = T_{BL}. \tag{6.1o}$$

6.1. *Matching stream with boundary layer*

The matching region between stream and boundary layer corresponds to $y_s \to -y_M(x_s, t)$ and $Y \to \infty$. We have shown that s_s and S are independent at leading order of y_s and Y, respectively. Matching surface elevation therefore requires that

$$S^{(0)}(x_s, t) = s_s(x_s, t), \tag{6.2}$$

which we may understand to mean that the ice thickness in the boundary layer is dictated by the thickness in the ice stream. Matching ice velocities in the matching region we get $u_s \sim \delta_s U^{(0)}$ for $\epsilon_s/\delta_s \lesssim 1$, $u_s \sim \epsilon_s(\delta_s/\epsilon_s)^{1/n} U^{(0)}$ for $\epsilon_s/\delta_s \gg 1$, $v_s \sim V^{(0)}$, and $w_s \sim \delta_s^{-1} W^{(0)}$, or at leading order

$$u_s|_{y_s = -y_M} = 0, \quad v_s|_{y_s = -y_M} = \lim_{Y \to \infty} V^{(0)}. \tag{6.3a,b}$$

Since $v_s = v_s(x_s, y_s, t)$ is independent of z_s, the second equation also implies that velocity $V^{(0)}$ has no vertical shear as $Y \to \infty$, so

$$W^{(0)} \to 0, \quad \frac{\partial V^{(0)}}{\partial Z} \to 0 \quad \text{as } Y \to \infty. \tag{6.4a,b}$$

Matching lateral shear stresses in the boundary layer requires $\tau_{xy,s} \sim \mathscr{T}_{xy}$, or

$$\lim_{Y \to \infty} \eta \frac{\partial U^{(0)}}{\partial Y} = \tau_M, \tag{6.5}$$

https://doi.org/10.1017/jfm.2015.503 Published online by Cambridge University Press

where for later convenience we define the lateral shear stress imposed by the stream on the margin as

$$\tau_M = \tau_{xy,s}(x_s, -y_M, t) = \frac{1}{2^{1/n}} \left| \frac{\partial u_s}{\partial y_s} \right|^{1/n-1} \frac{\partial u_s}{\partial y_s} \Bigg|_{y_s=-y_M}. \tag{6.6}$$

Matching temperatures and heat fluxes leads to $T_{BL} \sim T_s$, $\delta_s \partial T_s/\partial y_s \sim \partial T_{BL}/\partial Y$, or at leading order

$$T_s(x_s, -y_M, t) = \lim_{Y\to\infty} T_{BL}, \quad \lim_{Y\to\infty} \frac{\partial T_{BL}}{\partial Y} = 0. \tag{6.7a,b}$$

These matching conditions provide boundary conditions on the stream and boundary layer problems and we can understand them in terms of the equations they most readily apply to. For instance (6.3*a*) closes the ice stream flow problem (3.15), while (6.3*b*) couples mass conservation of the stream (3.18*c*) to the boundary layer. Conversely, (6.5) provides boundary conditions for the longitudinal Stokes flow problem in the boundary layer (5.17), while (6.4) provides the necessary boundary conditions for the transverse Stokes flow problem (5.20). Assuming there is net inflow of ice into the ice stream, $-v_s(x_s, -y_M, t) - \partial y_M/\partial t < 0$, (6.7*b*) helps to close the heat equation for the boundary layer (5.12), while (6.7*a*) acts as a boundary condition for the temperature in the stream.

6.2. *Matching boundary layer with ridge*

The matching region between ridge and boundary layer is at $Y \to -\infty$, $y_r \to 1 - (\epsilon_s/\epsilon_r)y_M$. Recall that ϵ_s/ϵ_r by definition is a scale for the half-width of the ice stream divided by the half-width of the domain, and must therefore be less than unity. There is the possibility that ϵ_s/ϵ_r is small, in which case the matching region at leading order is at a fixed position $y_r \to 1$, which however does not affect the matching procedure below.

When matching boundary layer and ice ridge, the ratio

$$\gamma = \frac{[z]_s}{[z]_r} = \frac{\epsilon_s \delta_s}{\epsilon_r \delta_r} \tag{6.8}$$

turns out to be of central importance. As a last constraint on our independent parameters ϵ_s, ϵ_r and δ_s we will assume in the procedure below that $\gamma \lesssim 1$, meaning that the natural ice ridge thickness is not less than the natural ice stream thickness, so ice in the ridge naturally wants to flow towards the ice stream. This constraint can be expressed as

$$\delta_s \lesssim \epsilon_s^{1/(n+1)} \epsilon_r^{n/(n+1)}. \tag{6.9}$$

This constraint is in addition to $\epsilon_s^{(2n+3)/(n+2)} \delta_s^{(n+1)/(n+2)} \ll \epsilon_r \ll 1$ from (4.3) and either $\epsilon_s \lesssim \delta_s$ or $\epsilon_s^{n+1} \ll \delta_s \ll \epsilon_s \ll 1$ from (5.1) and it is easy to see that these constraints are not mutually incompatible. With the typical parameter values from table 1, $\gamma \approx 0.9$, so our assumption of $\gamma \lesssim 1$ is reasonable. That being said, it is possible in principle to deal with the case $\gamma \gg 1$ through a rescaling of the ice ridge equations (Haseloff 2015).

The surface elevation in the boundary layer is flat at leading order, so that matching surface elevations leads to

$$s_r(x_s, 1 - (\epsilon_s/\epsilon_r)y_M, t) = \gamma S^{(0)}(x_s, t) = \gamma s_s(x_s, t) \tag{6.10}$$

https://doi.org/10.1017/jfm.2015.503 Published online by Cambridge University Press

by use of (6.2). It is also possible to match surface slopes, which however requires the next-order correction $S^{(1)}$.

Matching the velocities we either have $U^{(0)} \sim \epsilon_s^2 \delta_r^{-1} u_r$ for $\epsilon_s/\delta_s \lesssim 1$ or $U^{(0)} \sim \delta_s \delta_r^{-1} \epsilon_s (\epsilon_s/\delta_s)^{1/n} u_r$ for $\epsilon_s/\delta_s \gg 1$, $V^{(0)} \sim \gamma v_r$, and $W^{(0)} \sim \gamma \delta_r w_r$. To simplify the matching conditions for the transverse velocity components $V^{(0)}$ and v_r, we can combine (4.15*b*) and (4.17), so that

$$v_r = \frac{(n+2)}{(n+1)} \frac{q_r}{s_r} \left[1 - \left(1 - \frac{z_r}{s_r} \right)^{n+1} \right]. \tag{6.11}$$

With $s_r \sim \gamma S^{(0)}$, $z_r \sim \gamma Z$, this means that $\gamma v_r \sim V^{(0)}$ in the matching region can be expressed as

$$\lim_{Y \to -\infty} V^{(0)} = \frac{(n+2)}{(n+1)} \frac{q_M}{S^{(0)}(x_s, t)} \left[1 - \left(1 - \frac{Z}{S^{(0)}(x_s, t)} \right)^{n+1} \right], \tag{6.12}$$

and the far-field value of $V^{(0)}$ is of $O(1)$ provided the dimensionless ridge mass flux q_r at the margin is $O(1)$ (as it generally will be). Here we have introduced the shorthand

$$q_M = q_r(x_r, 1 - (\epsilon_s/\epsilon_r) y_M, t) \tag{6.13}$$

for the depth-integrated flux in the ridge at the margin. The other two velocity conditions in the matching region become

$$U^{(0)} \to 0, \quad W^{(0)} \to 0 \quad \text{as } Y \to -\infty. \tag{6.14a,b}$$

The matching conditions on boundary layer velocity (6.12) and (6.14) close the boundary layer flow problems (5.19) and (5.20).

Equation (6.10) shows that the boundary value for ice thickness in the ice ridge is set by the ice stream and provides one instance of direct coupling between stream and ridge, which provides the necessary boundary condition on (4.17) (as well as setting ice thickness in the boundary layer itself). We can further show that inflow into the stream is directly given by the value of ice flux into the stream at the boundary. We can integrate the continuity equation for the boundary layer, (5.20*c*), to show that

$$0 = \int_{Z=0}^{Z=S^{(0)}} \frac{\partial V^{(0)}}{\partial Y} \, \mathrm{d}Z + W|_{Z=0}^{Z=S^{(0)}} = \int_{Z=0}^{Z=S^{(0)}} \frac{\partial V^{(0)}}{\partial Y} \, \mathrm{d}Z \tag{6.15}$$

by use of the boundary conditions $W^{(0)} = 0$ at $Z = 0$ and $Z = S^{(0)}$, (5.21*a*) and (5.22). Further integration over the width of the boundary layer from $Y = -\infty$ to ∞, assuming that all the relevant limits commute, together with use of the matching conditions, yields

$$0 = \int_{Z=0}^{Z=S^{(0)}} \lim_{Y \to \infty} V^{(0)} \, \mathrm{d}Z - \int_{Z=0}^{Z=S^{(0)}} \lim_{Y \to -\infty} V^{(0)} \, \mathrm{d}Z = v_s(x_s, -y_M, t) s_s(x_s, t) - q_M \tag{6.16}$$

by use of (5.16), (6.3*b*), (6.12), and (3.9*e*). Together with (6.3*a*), this shows that the inflow of ice into the stream q_{in} in (3.18*c*) can be written in terms of the discharge of ice from the ice ridge q_M and the margin migration rate $\partial y_M/\partial t$ as

$$q_{in} = 2 s_s \frac{\partial y_M}{\partial t} + 2 q_M. \tag{6.17}$$

https://doi.org/10.1017/jfm.2015.503 Published online by Cambridge University Press

Finally, we need to match temperatures,

$$\lim_{Y\to-\infty} T_{BL}(X, Y, Z, t) = T_r(x_r, 1-(\epsilon_s/\epsilon_r)y_M, z_r, t). \tag{6.18}$$

This acts as an inflow boundary condition for the heat equation (5.12).

7. Solution of the boundary layer model

In terms of the mechanical and kinematic coupling between the ice stream and ice ridge flow models, the margin boundary layer turns out to be essentially passive. The ice ridge is coupled to the ice stream by having to match the ice stream surface height at the interface between the two, which becomes the relevant boundary condition for (4.16). Conversely, the ice stream velocity problem (3.15) has to satisfy a zero velocity boundary condition at the ice stream margins $y = \pm y_m$, while the stream couples to the ridge through continuity of flux, setting $q_{in} = 2s_s\partial y_M/\partial t + 2q_M$ in (4.17). We were able to obtain these intuitive results by matching stream to ridge across the boundary layer without actually having to solve the boundary layer equations.

By contrast, the boundary layer holds the key to computing the margin migration rate $\partial y_M/\partial t$. The problem for temperature T in the boundary layer (5.12), (5.13), (6.7) and (6.18) is nearly identical to the ice stream margin problem in Schoof (2012), and the latter predicts a unique solution for the margin migration rate as a function of various forcing parameters. The boundary layer model here generalizes Schoof's version through the addition of an advection term that accounts for transverse flow through the margin. Schoof's model is restricted to a widening ice stream with $\partial y_M/\partial t > 0$ (see, however, the appendix to Schoof's paper for a discussion of the opposite case). For a widening stream, it is necessary to add a constraint on heat fluxes on the ice stream side of the temperate–frozen transition at $Y = 0$:

$$-\frac{\partial T_{BL}}{\partial Z}\bigg|^{+} + \kappa\,\frac{\partial T_{BL}}{\partial Z}\bigg|^{-} \leqslant 0 \quad \text{for } Y > 0,\ \ Z = 0. \tag{7.1}$$

If this condition was violated, then as the ice stream widens the newly unfrozen bed would be subjected to net heat loss. At this point the bed should not yet contain any liquid water to freeze and would not remain unfrozen in contradiction to our assumption that the ice stream is widening. We adopt the same assumptions, adding the constraint (7.1) to the temperature constraint (5.13*e*) already in place on the temperate side of the cold–temperate transition at $Y = 0$.

We make one further expedient simplification here, which is not truly justified by our scale estimates: we treat the Péclet number Pe_{BL} as an $O(1)$ quantity. The realistic limit of large Péclet numbers can be dealt with in the framework we have developed, but this is somewhat involved and therefore beyond the scope of this paper. Our aim is to demonstrate how transverse flow affects the lateral migration rates computed by Schoof (2012), for which treating Pe_{BL} as $O(1)$ provides a useful first step. Similarly, we treat α_{BL} as $O(1)$.

In addition, we assume that $\epsilon_s/\delta_s \ll 1$ in the boundary layer model, which corresponds to the case of lateral shear stresses dominating over stresses generated by transverse inflow across the margin (see (5.6)). Even though our scale estimates suggest that ϵ_s is not much smaller than δ_s, a dominant lateral shear stress is actually the most realistic scenario for a real ice stream: the lateral shear stresses predicted by our scale estimates are somewhat smaller than those inferred from direct observations.

https://doi.org/10.1017/jfm.2015.503 Published online by Cambridge University Press

The limit of small ϵ_s/δ_s in principle should let us simplify viscosity and heat production rates as

$$\eta = \frac{1}{2^{1/n}}\left(\left|\frac{\partial U^{(0)}}{\partial Y}\right|^2 + \left|\frac{\partial U^{(0)}}{\partial Z}\right|^2\right)^{(1-n)/(2n)} \quad \text{and} \quad a = \frac{1}{2^{1/n}}\left(\left|\frac{\partial U^{(0)}}{\partial Y}\right|^2 + \left|\frac{\partial U^{(0)}}{\partial Z}\right|^2\right)^{(1+n)/(2n)}. \tag{7.2a,b}$$

However, in the case of the viscosity, omitting the $O(\epsilon_s^2/\delta_s^2)$ terms due to lateral inflow is problematic as the derivatives of $U^{(0)}$ vanish in the far field as $Y \to -\infty$. With $n > 1$, this leads to an infinite viscosity. In principle this can be fixed through the introduction of yet another (rather trivial and passive) boundary layer in which all the velocity gradients are of similar size, but it is in practice (especially numerically) simpler to retain the additional velocity gradients due to lateral inflow in the viscosity.

To close the temperature problem, we also assume that the temperature field in the matching region with the ridge can be treated as being piecewise linear, with the temperature gradient given by the geothermal heat flux:

$$\lim_{Y\to-\infty} T_{BL}(X, Y, Z, t) = \begin{cases} \nu_s(S^{(0)} - Z) - 1 & \text{for } 0 < Z < S^{(0)} \\ \nu_s\left(S^{(0)} - \dfrac{1}{\kappa}Z\right) - 1 & \text{for } Z < 0. \end{cases} \tag{7.3}$$

It turns out that this is formally the correct temperature solution for the ridge in the parameter regime we have just defined: from $Pe_r = \delta_r Pe_{BL}$ (see table 3), the ridge Péclet number is small if Pe_{BL} is of $O(1)$, while the ridge shear heating parameter α_r is also small: with $\alpha_r = (\epsilon_s/\delta_s)(\epsilon_s/\epsilon_r)^{1/(n+1)}\alpha_{BL}$ as well as $\epsilon_s/\epsilon_r = W_s/W < 1$ and $\epsilon_s/\delta_s \ll 1$, it follows that $\alpha_r \ll \alpha_{BL} = O(1)$. With small Pe_r and α_r, we obtain a linear temperature profile $T_r = \nu_r(s_r - z_r) - 1$ as solution of (4.13*a*). This is of course contrived, as Pe_{BL} and α_{BL} should not be treated as $O(1)$, and less trivial far-field temperature fields are possible in real ice sheets. As mentioned, these more complicated cases will be dealt with separately, and (7.3) for now provides a convenient, self-consistent closure to the boundary layer heat equation.

7.1. *A reduced problem*

Before we actually solve the boundary layer model, we restate it with the additional assumptions we have just made. It is convenient to introduce another rescaling at this stage, as this allows us to absorb quantities such as the dimensionless ice thickness, dimensionless inflow rate, and dimensionless lateral shear stress in the ice stream margin into a minimum number of dimensionless groups.

We define

$$(Y^*, Z^*) = \frac{(Y, Z)}{s_s}, \quad S^* = \frac{S^{(1)}}{s_s}, \quad P^* = \frac{P^{(1)}}{s_s}, \quad U^* = \frac{U^{(0)}}{\tau_M s_s}, \tag{7.4a–d}$$

$$(V^*, W^*) = \frac{(n+1)}{(n+2)}\frac{s_s}{q_M}(V^{(0)}, W^{(0)}), \quad T^* = T_{BL}. \tag{7.4e,f}$$

The ice flow problem in the boundary layer now takes the same mathematical form as (5.17), (5.19)–(5.22), but with the superscripts, specifically (0) on U, V, W and (1) on P and S, replaced by asterisks. The independent variables Y and Z in these

https://doi.org/10.1017/jfm.2015.503 Published online by Cambridge University Press

equations are likewise replaced by (Y^*, Z^*) under this procedure, and the upper surface is located at $Z^* = 1$. Our interest is in the limit $\epsilon_s \ll \delta_s$, but we retain the formula given by the first case of (5.18), with ϵ_s^2/δ_s^2 replaced by a small fixed value of 10^{-2} in order to avoid divergent viscosities in the far field; numerical experiments have shown the solution for $\partial y_M/\partial t$ to be insensitive to changes in the value of the regularizing parameter ϵ_s^2/δ_s^2 provided this is kept small.

The far-field boundary conditions in the meantime become

$$U^* \to 0, \quad V^* \to 1 - (1 - Z^*)^{n+1}, \quad W^* \to 0 \quad \text{as } Y^* \to -\infty, \tag{7.5a–c}$$

$$\eta \frac{\partial U^*}{\partial Y^*} \to 1, \quad \frac{\partial V^*}{\partial Z^*} \to 0, \quad W^* \to 0 \quad \text{as } Y^* \to \infty. \tag{7.5d–f}$$

Importantly, in this form, the ice flow problem becomes completely free of any parameters (other than the material constant n), and the strength of lateral inflow can be completely absorbed into a redefined Péclet number, as we see below.

With $Pe_{BL} = O(1)$ and δ_s small, the rescaled heat equation for the boundary layer takes the form

$$v_m \frac{\partial T^*}{\partial Y^*} + Pe\,(V^*, W^*) \cdot \boldsymbol{\nabla} T^* - \nabla^2 T^* = \alpha \frac{|\boldsymbol{\nabla} U^*|^{1+1/n}}{2^{1+1/n}} \quad \text{for } 0 < Z^* < 1, \tag{7.6a}$$

$$v_m \Gamma \frac{\partial T^*}{\partial Y^*} - \kappa \nabla^2 T^* = 0 \quad \text{for } Z^* < 0, \tag{7.6b}$$

where $v_m = Pe_{BL} s_s \partial y_M/\partial t$ is a proxy for the migration rate, and $\boldsymbol{\nabla} = (\partial/\partial Y^*, \partial/\partial Z^*)$ is the gradient operator in the transverse direction. Boundary conditions are

$$T^* = -1 \quad \text{at } Z^* = 1, \quad \lim_{Z^* \to -\infty} -\kappa \frac{\partial T^*}{\partial Z^*} \to \nu, \tag{7.7a,b}$$

$$\lim_{Y^* \to -\infty} T^* = \begin{cases} -1 - \nu(Z^* - 1) & \text{for } 0 < Z^* < 1 \\ -1 - \nu\left(\dfrac{1}{\kappa} Z^* - 1\right) & \text{for } Z^* < 0, \end{cases} \qquad \lim_{Y^* \to \infty} \frac{\partial T^*}{\partial Y^*} = 0, \tag{7.7c,d}$$

$$T^* < 0 \quad \text{and} \quad -\left.\frac{\partial T^*}{\partial Z^*}\right|^+ + \kappa \left.\frac{\partial T^*}{\partial Z^*}\right|^- = 0 \quad \text{for } Y^* < 0,\ Z^* = 0, \tag{7.7e,f}$$

$$T^* = 0 \quad \text{and} \quad -\left.\frac{\partial T^*}{\partial Z^*}\right|^+ + \kappa \left.\frac{\partial T^*}{\partial Z^*}\right|^- \leqslant 0 \quad \text{for } Y^* > 0,\ Z^* = 0. \tag{7.7g,h}$$

Our rescaling has led to a new Péclet number, heat production parameter and dimensionless heat flux appearing, related to their previous versions, and to dimensional parameters describing the near-margin behaviour of the ridge and stream through

$$Pe = Pe_{BL} \frac{(n+2)}{(n+1)} q_M = \frac{(n+2)}{(n+1)} \frac{\rho c Q_r}{k}, \quad \nu = \nu_s s_s = \frac{q_{geo} h_s}{k(T_m - T_0)}, \tag{7.8a,b}$$

$$\alpha = \alpha_{BL} \tau_M^{n+1} s_s^2 = 2 \frac{A \tau_s^{n+1} h_s^2}{k(T_m - T_0)}. \tag{7.8c}$$

https://doi.org/10.1017/jfm.2015.503 Published online by Cambridge University Press

Here h_s is the dimensional ice stream thickness, τ_s is the dimensional lateral shear stress in the ice stream at the margin, and Q_r is the dimensional ice flux from the ridge into the margin. Further, the dimensional margin migration rate V_m can be related to its dimensionless counterpart v_m through

$$V_m = \frac{k}{\rho c h_s} v_m. \tag{7.9}$$

If the boundary layer problem as stated admits a unique margin migration velocity v_m, then it follows that v_m can only depend on Pe, α and ν and the three material constants, κ, Γ and n. More specifically, the rescaling above suggests that, for a given set of material constants, the dimensional margin migration velocity V_m can be computed from the near-margin behaviour of ridge and stream as

$$V_m = \frac{k}{\rho c h_s} f\left(\frac{\rho c Q_r}{k}, \frac{A\tau_s^{n+1} h_s^2}{k(T_m - T_0)}, \frac{q_{geo} h_s}{k(T_m - T_0)}\right) \tag{7.10}$$

for some function f that still needs to be determined.

7.2. *Solution*

It remains to be shown that the boundary layer problem indeed furnishes a single solution for v_m given a set of parameters Pe, α, ν, κ, Γ and n. We are unable to give an actual proof here, but can note the following. The ice flow problem consists of a well-posed, coupled p-Laplacian and Stokes flow problem, to which analytical solutions have previously been found for the Newtonian case $n = 1$ (Barcilon & MacAyeal 1993; Schoof 2004, 2012). Given the resulting velocity field and dissipation rate, the (travelling wave) advection–diffusion-type heat equations (7.6) and (7.7) can be solved with any choice of v_m provided that we disregard the inequality constraints (7.7*e*) and (7.7*h*). However, with an arbitrary choice of v_m these inequalities are not guaranteed to be satisfied.

The work in Schoof (2012) shows that for no lateral inflow ($Pe = 0$) and with $\kappa = 1$, $\Gamma = 1$, there is a unique value of v_m for a given value of α and ν such that both inequality constraints are satisfied simultaneously. Migration velocities that are too small lead to a build-up of excessive heat as the margin position remains in place for longer. Temperatures at the bed on the ice ridge side then rise above the melting point, which is in violation of the inequality constraint (7.7*e*). Conversely, migration velocities that are too large lead to insufficient build-up of heat as the margin advances into the colder ice in the ice ridge. This causes freezing inside the stream bed, with singular freezing rates near the slip to no-slip transition. In this case, the constraint (7.7*h*) is violated.

These results appear to carry over to the case with lateral inflow ($Pe > 0$). We solve the boundary layer problem numerically using the finite element package Elmer/Ice (Gagliardini *et al.* 2013), reducing the semi-infinite domain to a large rectangle with the far-field conditions applied at the appropriate edges of the rectangle. For any given computational mesh and set of parameter values, we find that one of the two constraints (7.7*e*) and (7.7*h*) is violated except for v_m inside a narrow range. The size of that range shrinks with element size, which we take to imply that there is only a single migration velocity for which both inequality constraints are satisfied in the continuum limit (by which we mean the limit of a vanishing element size rather than the rather different concept of treating a polycrystalline aggregate as a continuum).

https://doi.org/10.1017/jfm.2015.503 Published online by Cambridge University Press

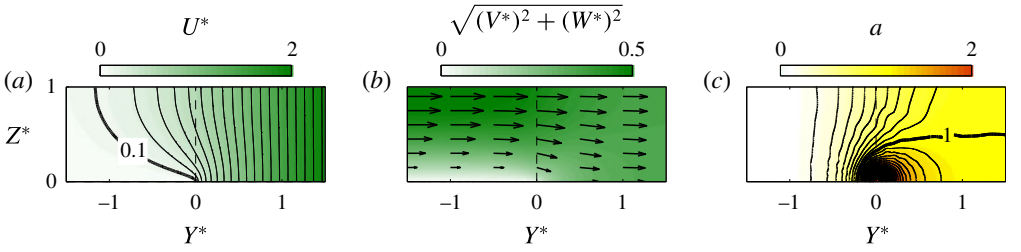


FIGURE 2. (Colour online) (*a*) Contours of axial velocity component U^* at contour intervals 0.1, with $U^* = 0.1$ shown as a bold line. (*b*) The transverse velocity field (V^*, W^*) shown as arrows, shading indicates magnitude of the transverse velocity. (*c*) Contours of heat production a at contour intervals 0.1, with $a = 1$ shown as a bold line. Note that contours of a are less smooth than those of U^* because the numerical error in ∇U^* is larger than the error in U^* itself, and the mesh used is locally refined near the origin but becomes coarser for larger distances. Only part of the computational domain is shown in each case.

In practice we use a bisection method to determine the migration speed v_m for a given set of parameter values. The upper limit of the search interval is a migration velocity that is too big and therefore violates (7.7*h*); the lower limit of the search interval violates (7.7*e*). As with a standard bisection method we halve the search interval at every iteration. We determine in which interval we continue the search from the inequality constraint that is violated at the midpoint: if (7.7*e*) is violated we continue in the upper half, otherwise in the lower half, and continue the process until a prescribed interval size is reached.

For comparison with previous work in Schoof (2012), the results we present here were computed with $\kappa = 1$, $\Gamma = 1$ and $n = 1$. In the discussion that follows, we also omit the asterisks on the rescaled variables for simplicity. Figure 2 shows a finite element solution of the flow problem in the boundary layer. The axial velocity U^* exhibits no vertical shear in the ice stream far field, but instead has a prescribed lateral gradient of $\eta \partial U^*/\partial Y^* \to 1$, as shown in figure 2(*a*), where contours are plotted in the (Y^*, Z^*) plane. There is intense shear around the transition from no slip to free slip at the origin, and the axial velocity goes to zero in the ice ridge far field. The intense shear around the origin translates to very high (in fact, singular) shear heating rates, $a = (1/4)|\nabla U^*|^2$, as shown in figure 2(*c*). The horizontal transverse velocity component V^* transitions from a shearing flow in the ice ridge to a plug flow in the ice stream, as shown in figure 2(*b*), while the vertical velocity component W^* is negative around the origin but vanishes in the far field.

A number of typical temperature fields are shown in figure 3, where we vary the heating parameter α at fixed $Pe = 0$ in figure 3(*a–c*), and vary the advection term Pe in figure 3(*d–f*) at a fixed heating rate α. As in Schoof (2012), increasing the heating rate leads to warmer temperatures on the ice stream side of the boundary layer. This is accompanied by faster migration velocities v_m that ensure that the bed temperature on the ridge side of the domain does not reach the melting point. These faster migration velocities turn out to lower temperatures in the bed and in the ice on the ridge side, as the margin migrates faster and parts of the domain away from regions of high dissipation do not have time to warm up to the same extent as for lower v_m. Conversely, if we add advective heat transport at constant dissipation rates, temperatures in the ice drop as dissipated energy is transported towards the ice stream

https://doi.org/10.1017/jfm.2015.503 Published online by Cambridge University Press

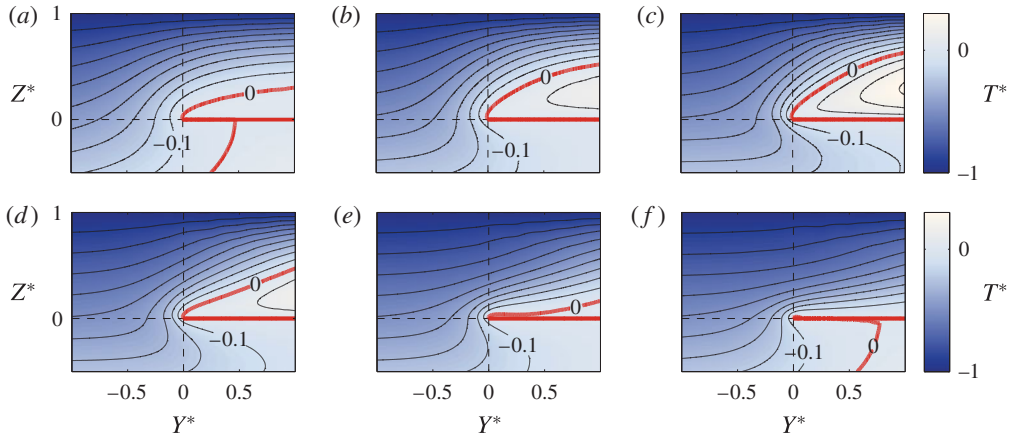


FIGURE 3. (Colour online) Temperature solutions at contour intervals of 0.1, with $T^* = 0$ shown as bold red line: (*a–c*) $Pe = 0$ and (*a*) $\alpha = 3$, (*b*) $\alpha = 5$, (*c*) $\alpha = 9$; (*d–f*) $\alpha = 9$ and (*d*) $Pe = 10$, (*e*) $Pe = 30$, (*f*) $Pe = 50$. All calculations were done with $\nu = 0.5$, and again only part of the computational domain is shown.

with the flow of the ice. The effect is most pronounced in the upper parts of the ice, where advection velocities are larger. In order to prevent the cooling of the ice from causing freezing at the bed on the ice stream side ($Y^* > 0$), an increase in advection velocities leads to smaller migration velocities, which in turn actually allows for warmer bed temperatures.

Note that each of the temperature fields shown has some region in which $T^* > 0$ in the ice, which is a feature of all the solutions we have computed (see also Schoof 2012). It implies that temperate ice – where ice reaches the melting point and a mixture of water and ice forms – must be present in the margins of a widening ice stream, even if the extent of temperate ice predicted by our model becomes small for large advection rates Pe (see figure 3*f*). Our model at this point assumes that the same heat equation can be used to model the specific energy content of temperate ice as for cold ice. This is a very special and not necessarily realistic case of an enthalpy gradient model for temperate ice (Aschwanden *et al.* 2012). We persist with it for now to facilitate comparison with prior work.

Figure 4 confirms the qualitative observations made above about the effect of heat production rate α and advection rate Pe on the migration velocity. Figure 4(*a*) shows the migration rate v_m against $\alpha/(1-\nu)$ at $Pe = 0$. Here, migration velocities are positive (meaning, that our assumption of a widening ice stream is satisfied) provided α exceeds some minimum value, and v_m increases with $\alpha/(1-\nu)$. The solution for v_m for the case of no advection, including the fact that v_m depends on α and ν only through the ratio $\alpha/(1-\nu)$, was previously found by Schoof (2012), and we use the semi-analytical Wiener–Hopf result from that earlier work primarily to confirm the accuracy of our numerical method. Clearly, very small element sizes are needed for accurate results (locally refined elements with edge lengths around 2.5×10^{-6} were necessary near the origin to reduce the error below 1 %), which can probably be ascribed to the high concentration of shear heating near the origin. All other computations reported here were done with similar or higher mesh resolutions.

Figure 4(*b*) shows that, when advection is added to the picture, migration speed still increases with α, but larger advection rates Pe lead to lower migration velocities

https://doi.org/10.1017/jfm.2015.503 Published online by Cambridge University Press

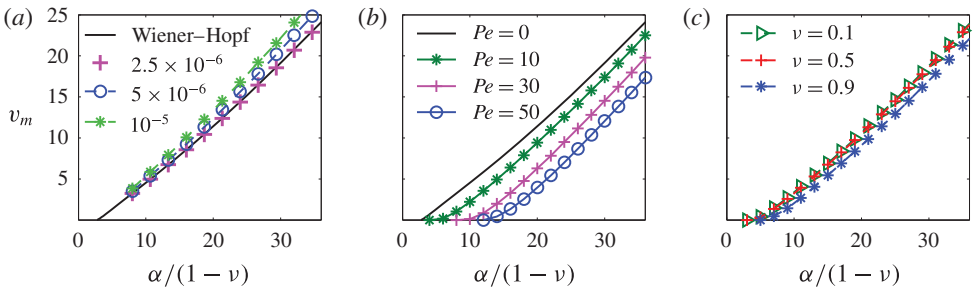


FIGURE 4. (Colour online) (*a*) Comparison of numerical results for varying minimal mesh resolutions and semi-analytical results for no advection. Calculations were done with $Pe = 0$ and $\nu = 0.25$. (*b*) Effect of adding advection; simulations for $\nu = 0.5$. (*c*) Solutions for $Pe = 10$ and different values of ν.

and a slight increase in the minimum dissipation rate needed to cause widening of the ice stream. In the presence of advection, it can be shown that v_m depends on α and ν separately, and not only through the ratio $\alpha/(1-\nu)$. This is easy to show by substituting a reduced temperature $\Theta = T^*/(1-\nu) + 1 + \nu Z^*/(1-\nu)$ into (7.6): when $Pe = 0$, then α and ν appear in the equivalent of (7.6) and (7.7) only as $\alpha/(1-\nu)$, while this is not the case when $Pe \neq 0$. In figure 4(*c*), we explore how sensitive v_m is to changes in ν when the ratio $\alpha/(1-\nu)$ is held constant. Note that ν has to lie in the interval $[0, 1)$ in order for the bed under the ridge not to reach the melting point as a result of geothermal heat flux alone, and within this range, we observe only slight variations in v_m when $\alpha/(1-\nu)$ is held constant. The latter combination of parameters can also be written in terms of dimensionless quantities as

$$\frac{\alpha}{1-\nu} = \frac{2A\tau_s^{n+1}h_s^2}{k(T_m - T_b)}, \tag{7.11}$$

where $T_b = T_0 + q_{geo}h_s/k$ is the far-field temperature at the bed in the matching region with the ridge. It therefore appears that margin migration velocity is primarily dependent on the difference between that far-field bed temperature and the melting point rather than on the details of the temperature gradient in the ice. This becomes relevant in the case of large Péclet numbers, where the temperature gradient in the ice need no longer be constant, and we will confirm that the migration rate is controlled primarily by the far-field bed temperature in a separate paper (Haseloff *et al.*, in preparation).

8. Discussion and conclusions

In this paper, we have developed two closely related models, both summarized in § 7.1. The first is a mechanical boundary layer description of the junction between the slow shearing flow of an ice ridge and a rapidly sliding, lateral-stress-dominated plug flow of an ice stream. The second is a model for the migration of that junction as a result of heat dissipation in the ice stream margin. Both models are based on the assumption that the margin of an ice stream coincides with a switch from a well-lubricated bed at the melting point, where rapid sliding is possible, to a frozen bed where no slip occurs. This does not preclude the possibility that the margins of some ice streams could be fixed by other means, for instance abrupt changes in subglacial

https://doi.org/10.1017/jfm.2015.503 Published online by Cambridge University Press

water pressure (Kyrke-Smith *et al.* 2014) or more exotic multiple-valued sliding laws (Sayag & Tziperman 2011).

Our mechanical boundary layer consists of a weakly coupled version of the model for lateral-stress-driven shearing in an idealized ice stream shear margin in Schoof (2004, 2012) and the model for ice flow across the equally idealized upstream onset of an ice stream in Barcilon & MacAyeal (1993), although in our case the geometry is somewhat different from that in Barcilon and MacAyeal's work (and therefore so are the far-field boundary conditions, in particular on the surface perturbation $S^{(1)}$). The weak coupling between the two flow problems in the boundary layer comes about through the strain-rate-dependent viscosity we have assumed, while the models in Schoof (2004, 2012) and Barcilon & MacAyeal (1993) were formulated for the Newtonian case. The margin migration model in turn is a generalized form of that in Schoof (2012), which we re-derive from first principles in the process of constructing the boundary layer model, and to which we add lateral advection of heat due to inflow of ice from the ridge into the stream.

The mechanical boundary layer model provides a self-consistent way of deriving the appropriate jump conditions between ridge and stream at the ice stream margin, which turn out to be the rather intuitive continuity of ice flux and ice thickness, as well as zero axial ice stream velocity at the margin. This generalizes the *ad hoc* formulation of jump conditions in prior work that couples leading-order ridge and stream models (e.g. Hulbe & MacAyeal 1999; Ritz, Rommelaere & Dumas 2001). There is, however, a caveat here: we have explicitly required the ice stream and ice ridge to be narrow as well as shallow in developing the boundary layer model, while the papers cited above do not. The main difference this leads to is that the velocity field solved for in Hulbe & MacAyeal (1999) and Ritz *et al.* (2001) is two-dimensional, while ours consists only of the axial velocity u_s in (3.15), with the cross-stream velocity field v_s a higher-order correction. A two-dimensional extension to the elliptic problem (3.15) naturally requires a second boundary condition. One might assume that continuity of depth-integrated normal velocity across the stream margin fixes the problem.

Making that assumption, however, turns out to be non-trivial: the narrowness of our ice stream is crucial to ensuring that normal stresses at the ice stream margin remain small relative to hydrostatic (or 'cryostatic') stresses, which is fundamental to our boundary layer model. Technically, it allows a parameter regime in which the relevant stress ratio λ defined in § 5 is small. For ice streams that are not narrow, normal stress will typically be comparable to cryostatic stresses, and the stress balance becomes similar to that at a marine ice sheet grounding line in which the grounded sheet does not slide (Chugunov & Wilchinsky 1996; Nowicki & Wingham 2008; Fowler 2011, chapter 10.2): slopes in the boundary layer will be $O(1)$, and the ice stream will be much thinner than the ice ridge, so continuity of ice thickness need no longer be the appropriate jump condition, and the boundary layer problem becomes harder to solve.

The extension of our model to the migration of ice stream margins is based on solving the heat equation in the boundary layer, requiring the migration velocity to be rapid enough so that the part of the bed that is subject to a no-slip boundary condition does not reach the melting point, while also requiring it to be slow enough not to cause freezing on the part of the bed where sliding does occur. As in Schoof (2012), we find that there is a single migration velocity that satisfies both of these constraints for any given set of forcing parameters, at least within what appears to be numerical error. Our boundary layer model puts Schoof's work on a more solid foundation, and further generalizes it to take account of heat transport due to lateral inflow of cold ice from the ice ridges. We find that this inflow significantly suppresses temperatures in the margin and reduces migration velocities.

https://doi.org/10.1017/jfm.2015.503 Published online by Cambridge University Press

There are several complications to the margin migration model that we will address in separate papers. In our model formulation, we have treated the Péclet number in the margin as being $O(1)$, whereas in reality it should be large, indicating that diffusion is ineffective over most of the boundary layer domain: this is equivalent to the contention in Fowler (2013) that Schoof's margin migration model requires a pseudo-steady temperature field to be established in the margin due to diffusion alone, which requires very long time scales. In a separate paper (Haseloff *et al.*, in preparation), we will show how the boundary layer model can be adapted to the case of large Péclet numbers. In addition, we have assumed that there is an abrupt transition from slip to no slip, which introduces a questionable singularity into the stress and shear heating fields, which partly explains the need for a very high mesh resolution in our numerical solutions, and can be alleviated by permitting at least a small amount of sliding on the 'frozen' side of the margin. Similarly, the additional physics introduced by the formation of temperate ice (in which the temperature reaches the melting point within the domain, see e.g. Suckale *et al.* 2014) have also been ignored in this paper. We will address both of these complications in detail elsewhere. A further complication that we have omitted from this work is the temperature-dependence of ice viscosity: at its most extreme, this could lead to effectively shear-weakening behaviour of the near-marginal ice, when depth-averaged (Perol *et al.* 2015).

We conclude by noting that the need for a boundary layer description may not be obvious in view of the types of models that underpin modern numerical ice sheet simulations. Many of these have moved away from coupling leading-order, lubrication-type 'shallow ice' models for ridges to membrane-type 'shallow stream' models across ice stream margins, and employ a hybrid formulation using so-called 'higher-order' models that can be applied regardless of how fast the ice sheet slides (Pattyn 2003; Bueler & Brown 2009; Cornford *et al.* 2013; Kyrke-Smith *et al.* 2013). These are, however, still thin-film models that do not apply in regions where the velocity field changes by $O(1)$ over a single ice thickness (Schoof & Hindmarsh 2010), and therefore cannot be relied on to describe the physics of the stream–ridge boundary layer. Naturally, this restriction does not apply to models that either solve the Stokes equations in the entire domain (Gillet-Chaulet *et al.* 2012), or adaptively determine the location of localized high-shear zones in which the Stokes equations must be solved instead of a higher-order model (Seroussi *et al.* 2012). However, while these approaches may handle the mechanical aspects of an ice stream shear margin adequately, it is still unlikely that they would be capable of solving our margin migration problem in practice: in order to reproduce known solutions to the margin migration problem, we found mesh resolutions around 10^{-6} times the ice thickness to be necessary near the transition from a frozen to a temperate bed. It is unlikely that such resolutions would be feasible even locally in large-scale ice sheet simulations, and a separate solution to the boundary layer problem seems more promising, computing margin migration velocity as a function of forcings imposed by ridge and stream.

Acknowledgements

We thank two anonymous referees and the editor Grae Worster for their constructive comments. M.H. acknowledges financial support through a Four Year Fellowship at the University of British Columbia (UBC) and Natural Sciences and Engineering Research Council of Canada (NSERC) grant no. 357193-13. C.S. was supported by

https://doi.org/10.1017/jfm.2015.503 Published online by Cambridge University Press

NSERC grants 357193-13 and 446042-13 and a Killam Faculty Research Fellowship at UBC. Numerical calculations on WestGrid equipment were supported by Compute Canada.

REFERENCES

ASCHWANDEN, A., BUELER, E., KHROULEV, C. & BLATTER, H. 2012 An enthalpy formulation for glaciers and ice sheets. *J. Glaciol.* **58**, 441–457.

BARCILON, V. & MACAYEAL, D. R. 1993 Steady flow of a viscous ice stream across a no-slip/free-slip transition at the bed. *J. Glaciol.* **39**, 167–185.

BUELER, E. & BROWN, J. 2009 The shallow shelf approximation as a sliding law in a thermomechanically coupled ice sheet model. *J. Geophys. Res.* **114**, F03008.

CATANIA, G., HULBE, C., CONWAY, H., SCAMBOS, T. A. & RAYMOND, C. F. 2012 Variability in the mass flux of the Ross ice streams, West Antarctica, over the last millennium. *J. Glaciol.* **58**, 741–752.

CHUGUNOV, V. A. & WILCHINSKY, A. V. 1996 Modelling of a marine glacier and ice-sheet-ice-shelf transition zone based on asymptotic analysis. *Ann. Glaciol.* **23**, 59–67.

CONWAY, H., CATANIA, G., RAYMOND, C. F., GADES, A. M., SCAMBOS, T. A. & ENGELHARDT, H. 2002 Switch of flow direction in an Antarctic ice stream. *Nature* **419**, 465–467.

CORNFORD, S. L., MARTIN, D. F., GRAVES, D. T., RANKEN, D. F., LE BROCQ, A. M., GLADSTONE, R. M., PAYNE, A. J., NG, E. G. & LIPSCOMB, W. H. 2013 Adaptive mesh, finite volume modeling of marine ice sheets. *J. Comput. Phys.* **232**, 529–549.

CREYTS, T. T. & SCHOOF, C. G. 2009 Drainage through subglacial water sheets. *J. Geophys. Res.* **114**, F04008.

CUFFEY, K. M., CONWAY, H., HALLET, B., GADES, A. M. & RAYMOND, C. F. 1999 Interfacial water in polar glaciers and glacier sliding at −17 °C. *Geophys. Res. Lett.* **26** (6), 751–754.

ECHELMEYER, K. A. & HARRISON, W. D. 1999 Ongoing margin migration of Ice Stream B, Antarctica. *J. Glaciol.* **45**, 361–369.

ENGELHARDT, H. & KAMB, B. 1997 Basal hydraulic system of a West Antarctic ice stream: constraints from borehole observations. *J. Glaciol.* **43**, 207–230.

ENGELHARDT, H. & KAMB, B. 1998 Basal sliding of Ice Stream B, West Antarctica. *J. Glaciol.* **44**, 223–230.

FOWLER, A. C. 1986 Sub-temperate basal sliding. *J. Glaciol.* **32**, 3–5.

FOWLER, A. C. 1987 Sliding with cavity formation. *J. Glaciol.* **33**, 255–267.

FOWLER, A. C. 2011 *Mathematical Geoscience*, Interdisciplinary Applied Mathematics, vol. 36. Springer Science & Business Media.

FOWLER, A. C. 2013 The motion of ice stream margins. *J. Fluid Mech.* **714**, 1–4.

FOWLER, A. C. & LARSON, D. A. 1978 On the flow of polythermal glaciers. I. Model and preliminary analysis. *Proc. R. Soc. Lond.* A **363** (1713), 217–242.

GAGLIARDINI, O., COHEN, D., RÅBACK, P. & ZWINGER, T. 2007 Finite-element modeling of subglacial cavities and related friction law. *J. Geophys. Res.* **112**, F02027.

GAGLIARDINI, O., ZWINGER, T., GILLET-CHAULET, F., DURAND, G., FAVIER, L., FLEURIAN, B., DE GREVE, R., MALINEN, M., MARTÍN, C., RÅBACK, P., RUOKOLAINEN, J., SACCETTINI, M., SCHÄFER, M., SEDDIK, H. & THIES, J. 2013 Capabilities and performance of Elmer/Ice, a new generation ice-sheet model. *Geosci. Model Develop.* **6**, 1299–1318.

GILLET-CHAULET, F., GAGLIARDINI, O., SEDDIK, H., NODET, M., DURAND, G., RITZ, C., ZWINGER, T., GREVE, R. & VAUGHAN, D. G. 2012 Greenland ice sheet contribution to sea-level rise from a new-generation ice-sheet model. *Cryosphere* **6**, 1561–1576.

HASELOFF, M. 2015 Modelling the migration of ice stream margins. PhD thesis, The University of British Columbia. Retrieved from http://hdl.handle.net/2429/54268.

HULBE, C. L. & MACAYEAL, D. R. 1999 A new numerical model of coupled inland ice sheet, ice stream, and ice shelf flow and its application to the West Antarctic Ice Sheet. *J. Geophys. Res.* **104**, 25349–25366.

https://doi.org/10.1017/jfm.2015.503 Published online by Cambridge University Press

HUPPERT, H. E. 1982 The propagation of two-dimensional and axisymmetric viscous gravity currents over a rigid horizontal surface. *J. Fluid Mech.* **121**, 43–58.

HUTTER, K. & OLUNLOYO, V. O. S. 1980 On the distribution of stress and velocity in an ice strip, which is partly sliding over and partly adhering to its bed, by using a Newtonian viscous approximation. *Proc. R. Soc. Lond.* A **373** (1754), 385–403.

IKEN, A. & BINDSCHADLER, R. A. 1986 Combined measurements of subglacial water pressure and surface velocity of Findelengletscher, Switzerland: conclusions about drainage system and sliding mechanism. *J. Glaciol.* **32**, 101–119.

IVERSON, N. R., BAKER, R. W., LEB HOOKE, R., HANSON, B. & JANSSON, P. 1999 Coupling between a glacier and a soft bed: I. A relation between effective pressure and local shear stress determined from till elasticity. *J. Glaciol.* **45**, 31–40.

JACOBSON, H. P. & RAYMOND, C. F. 1998 Thermal effects on the location of ice stream margins. *J. Geophys. Res.* **103**, 12111–12122.

JOUGHIN, I., TULACZYK, S., BINDSCHADLER, R. & PRICE, S. F. 2002 Changes in west Antarctic ice stream velocities: Observation and analysis. *J. Geophys. Res.* **107** (B11), 2289.

KAMB, B. 2001 Basal zone of the West Antarctic ice streams and its role in lubrication of their rapid motion. In *The West Antarctic Ice Sheet: Behaviour and Environment* (ed. R. B. Alley & R. A. Bindschadler), Antarctic Research Series, vol. 77, pp. 157–199. American Geophysical Union.

KYRKE-SMITH, T. M., KATZ, R. F. & FOWLER, A. C. 2013 Stress balances of ice streams in a vertically integrated, higher-order formulation. *J. Glaciol.* **59**, 449–466.

KYRKE-SMITH, T. M., KATZ, R. F. & FOWLER, A. C. 2014 Subglacial hydrology and the formation of ice streams. *Proc. R. Soc. Lond.* A **470** (2161), doi:10.1098/rspa.2013.0494.

MACAYEAL, D. R. 1989 Large-scale ice flow over a viscous basal sediment – theory and application to ice stream B, Antarctica. *J. Geophys. Res.* **94**, 4071–4087.

MOORE, P. L., IVERSON, N. R. & COHEN, D. 2010 Conditions for thrust faulting in a glacier. *J. Geophys. Res.* **115**, F02005.

MORLAND, L. W. & JOHNSON, I. R. 1980 Steady motion of ice sheets. *J. Glaciol.* **25**, 229–246.

MUSZYNSKI, I. & BIRCHFIELD, G. E. 1987 A coupled marine ice-stream–ice-shelf model. *J. Glaciol.* **33**, 3–15.

NOWICKI, S. M. J. & WINGHAM, D. J. 2008 Conditions for a steady ice sheet-ice shelf junction. *Earth Planet. Sci. Lett.* **265** (1), 246–255.

PATERSON, W. S. B. 1994 *The Physics of Glaciers*. Elsevier.

PATTYN, F. 2003 A new three-dimensional higher-order thermomechanical ice sheet model: basic sensitivity, ice stream development, and ice flow across subglacial lakes. *J. Geophys. Res.* **108**, 2382.

PAYNE, A. J. & DONGELMANS, P. W. 1997 Self-organization in the thermomechanical flow of ice sheets. *J. Geophys. Res.* **102**, 12219–12234.

PEROL, T., RICE, J. R., PLATT, J. D. & SUCKALE, J. 2015 Subglacial hydrology and ice stream margin locations. *J. Geophys. Res.* **120**, 1352–1368.

RAYMOND, C. 1996 Shear margins in glaciers and ice sheets. *J. Glaciol.* **42**, 90–102.

RIGNOT, E., MOUGINOT, J. & SCHEUCHL, B. 2011 Ice flow of the antarctic ice sheet. *Science* **333** (6048), 1427–1430.

RITZ, C., ROMMELAERE, V. & DUMAS, C. 2001 Modeling the evolution of Antarctic ice sheet over the last 420 000 years: implications for altitude changes in the Vostok region. *J. Geophys. Res.* **106**, 31943–31964.

SAYAG, R. & TZIPERMAN, E. 2011 Interaction and variability of ice streams under a triple-valued sliding law and non-Newtonian rheology. *J. Geophys. Res.* **116**, F01009.

SCHOOF, C. 2004 On the mechanics of ice-stream shear margins. *J. Glaciol.* **50**, 208–218.

SCHOOF, C. 2005 The effect of cavitation on glacier sliding. *Proc. R. Soc. Lond.* A **461** (2055), 609–627.

SCHOOF, C. 2012 Thermally driven migration of ice-stream shear margins. *J. Fluid Mech.* **712**, 552–578.

SCHOOF, C. & HEWITT, I. 2013 Ice-sheet dynamics. *Annu. Rev. Fluid Mech.* **45**, 217–239.

https://doi.org/10.1017/jfm.2015.503 Published online by Cambridge University Press

SCHOOF, C. & HINDMARSH, R. C. A. 2010 Thin-film flows with wall slip: an asymptotic analysis of higher order glacier flow models. *Q. J. Mech. Appl. Maths* **63** (1), 73–114.

SEROUSSI, H., BEN DHIA, H., MORLIGHEM, M., LAROUR, E., RIGNOT, E. & AUBRY, D. 2012 Coupling ice flow models of varying orders of complexity with the Tiling method. *J. Glaciol.* **58**, 776–786.

SUCKALE, J., PLATT, J. D., PEROL, T. & RICE, J. R. 2014 Deformation-induced melting in the margins of the West Antarctic ice streams. *J. Geophys. Res.* **119**, 1004–1025.

https://doi.org/10.1017/jfm.2015.503 Published online by Cambridge University Press